Seasonal stages of chlorophyll-a vertical distribution and its relation to the light conditions in the Black sea from Bio-Argo measurements

Kubryakov[1] A.A., Mikaelyan A.S.[2], Stanichny S.V[1], Kubryakova E.A.[1]

[1]Marine Hydrophysical Institute, Russian Academy of Sciences, 2, Kapitanskaya str., Sevastopol, 299011, Russia

[2]Shirshov Institute of Oceanology, Russian Academy of Sciences, 36, Nakhimovski prosp., Moscow, 117997, Russia

Abstract

The year-to-year seasonal variability of the vertical distribution of chlorophyll-a (Chl), its relation with light conditions and mixing were studied in the Black Sea on a basis of 5-year (2014-2018) measurements of four Bio-Argo buoys. It was shown that the dependence of Chl on the logarithm of the instantaneous Photosynthetically Available Radiation (PAR) at noon (Ed), has quasigaussian shape. The majority of Chl values were in Ed interval from 3 to 330 μmol photons m^{-2} s^{-1} with a maximum at 20 μmol photons m^{-2} s^{-1}. During all seasons the high values of Chl were located above the Ed of 3 μmol photons m^{-2} s^{-1} or daily integrated PAR of 0.08 mole photons m^{-2} d^{-1}. This isolume can be regarded as a value close to compensational irradiance for the Black Sea phytoplankton restricting the productive layer. Low Chl observed at high Ed > 330 μmol photons m^{-2} s^{-1} evidences about important role of photoadaptaition and non-photochemical quenching in phytoplankton cells defining the amount of Chl in surface layer. In turn, Chl largely determines light conditions in the deep layers by modulating attenuation coefficient of PAR (Kd) and the dependence of Kd on Chl is well described by obtained in a study power function. In the study we described the seasonal variability in vertical distribution of Ed and presented the monthly averaged values of Kd in 5 m bins. Further, analysis of Bio-Argo data allows to distinguish 7 different stages of Chl annual succession in the basin. They are: 1) winter minimum; 2) March early-spring peak; 3) April-May depth-averaged minimum and the deepest Chl peak; 4) increased Chl in the thermocline in the second part of May and June; 5) large deep Chl peak in August; 6) early autumn depth-averaged minimum in September-October; 7) late autumn-early winter bloom in November-January. The roles of different abiotic and biotic factors (mixing, cross-shelf transport, illumination, light attenuation, phytoplankton growth rate limitation, grazing) in the formation of each of these stages are discussed.

1. Introduction

One of the main characteristics of the marine ecosystem is the vertical distribution of chlorophyll-a concentration (*Chl*), which is a proxy of phytoplankton abundance and reflects the level of primary production in the basin (Demidov, 2009; Finenko et al., 2005, 2009; Yunev, 2011). Vertical variability of the phytoplankton characteristics in the Black Sea was analyzed basing on field data in a large amount of studies. Many of them were dedicated to the estimation of the season cycle of the phytoplankton biomass, *Chl* and primary production, regional features of these characteristics and their dependence on different physical factors (Sorokin, 1983; Zernova, Nezlin, 1983; Vedernikov, Demidov, 1993; Mikaelyan, 1997; Demidov, 1999, 2008; Berseneva et al.,2004; Finenko et al., 2005; Stelmah, 2006; Krivenko, 2010; Krivenko, Parhomenko, 2011; Mikaelyan et al., 2011, 2018; Silkin et al., 2018). It was shown that column-averaged *Chl* have generally three seasonal maximums (winter-early spring, summer, autumn) (Vedernikov, Demidov, 1993; Demidov, 1999; Finenko et al., 2005; Krivenko, 2010; Kubryakova et al., 2018), while surface *Chl* is characterized by two maxima in late autumn and early spring (Berseneva et al., 2004; Demidov, 2009; Krivenko, Parhomenko, 2010). General feature of *Chl* vertical distribution is deepening of peak during warm period of a year and a formation of a so-called deep chlorophyll maximum (Sorokin, 1983; Vedernikov, Demidov, 1993), similarly as in the other areas of the World Ocean at the same latitudes. The variability of the thickness, depth and shape of summer deep maximum in the Black Sea were investigated in details in (Finenko et al., 2005; Krivenko, 2010).

Satellite scanners provide a large amount of data about spatial-temporal variability of surface *Chl* (Kopelevich et al., 2002; Nezlin, 2008; Finenko et al., 2014; Kubryakov et al., 2016). Particularly, they give information about the importance of the impact of the mesoscale eddy dynamics on the cross-shelf fluxes of nutrients and *Chl* to the deep part of the basin (Oguz et al., 2002; Shapiro et al., 2009; Kubryakov et al., 2016). Satellite *Chl* data helped to reveal the key role of the temporal water stratification in the winter pulsing blooms of phytoplankton (Mikaelyan et al., 2017a). Modis satellite scanner measurements of *Chl* together with Bio-Argo data showed the strong impact of storms on the development of anomalous blooms of phytoplankton in the warm period of a year (Kubryakov et al., 2019a). Long-term analysis of satellite and in-situ data showed that seasonal surface peak of *Chl* is controlled by river discharge in the shelf areas and by start of winter convection in the deep areas of the basin (Krivenko, Parhomenko, 2010; Finenko et al., 2014; Kubryakova et al., 2018). Unfortunately, satellite data give information only about surface variability and they are unable to elucidate the important features of *Chl* seasonal dynamics, such as its subsurface maximum.

Although field measurements give results on the variability of the vertical distribution of *Chl*, usually, they have a rather rough resolution 5-15 meters. Having in mind a thin vertical structure of *Chl* in the ocean (Mankovsky et al., 2010; see review in Durham, Stoker, 2012), such low vertical resolution can lead to the smoothing of the main vertical features of phytoplankton distribution, especially in the zones of the sharp changes of *Chl* and physical characteristics, i.e. near thermocline or pycnocline.

Another important problem is a lack of simultaneous continuous measurements of light parameters (downwelling irradiance, diffuse attenuation) and phytoplankton characteristics. Although the data on the seasonal changes of the euphotic layer was obtained in several studies (Vedernikov, Demidov, 1993; Demidov, 1999; Finenko et al., 2002), the detailed joint analysis of vertical profiles of irradiance and *Chl* is almost absent in the Black Sea. Optical characteristics of the Black Sea waters were studied in several in-situ studies (Vladimirov et al., 1997; Churilova, 2004; 2008; 2009, 2017; Mankovsky et al., 2010). However, due to the lack of continuous measurements, especially in recent years, the data on seasonal variability in vertical distribution of light attenuation coefficients are very restricted.

Despite the relation of light, the mixed layer depth (MLD) and spring phytoplankton blooms was firstly described by (Gran and Braarud 1935; Sverdrup, 1953), until now there are large debates on some crucial questions. Particularly, recent findings reveal that the classical definition of the euphotic depth as 1% of surface Photosynthetically Available Irradiance (PAR) does not define the real thickness of the productive layer (Banse, 2004; Letelier et al., 2004). The primary production and high *Chl* can occur either higher or lower than this border (see e.g. Letelier et al., 2004; Mara et al., 2014). In the Black Sea, in several classical works the value of 0.1% of surface PAR instead of 1% was used for the definition of the photic zone (Vedernikov, Demidov, 1993; Demidov, 1999). Still, there are evidences that rather high amount of phytoplankton can be observed as just above, as below of this border (0.1% of surface PAR) (Demidov, 1999).

Another important question is the mechanism of the early spring phytoplankton bloom. Recently, studies have shown that the classical model relating the spring bloom to the mixed layer shallowing sometimes does not work, e.g. in the Northern Atlantic (Boss, Behrenfield, 2010; Ferrari et al., 2015). Instead, the authors showed that spring bloom starts when the wind turbulent mixing becomes negligible that stops mixing in the upper mixed layer, which thickness can be still large (Taylor, Ferrari, 2011; Ferrari et al., 2015). Further, in this article, we will show that in the Black Sea the different case is observed – spring bloom develops both inside and under the mixed layer, and its vertical expansion is controlled, first of all, by an increase in downwelling irradiance.

Another issue, which was only briefly mentioned in the Black Sea (Sorokin, 1980; Vedernikov, Demidov, 1993) is the impact of the high insolation on the *Chl* seasonal dynamics in the upper layers, through photoinhibition mechanisms. Photoadaptive behavior of phytoplankton plays the important role in its seasonal variability, especially in summer months (Finenko et al., 2002, 2005; Churilova et al., 2009, 2017). This photoinhibition/phodoadaptaion can be crucial for the *Chl* dynamics in the upper layers, as it was demonstrated recently for the South Ocean (Alderkamp et al., 2010, 2011; Xing et al., 2019).

Therefore, despite large previous efforts there are still significant gaps in the current understanding of the variability of *Chl* and its relation to the physical factors, especially irradiance on seasonal time scales. One of the important reasons of these gaps is the absence of continuous measurements of the biooptical properties. The recent deployment of the Bio-Argo floats gives a possibility to overcome this problem (Claustre et al., 2010). Bio-Argo buoys today gives simultaneous information about several key biooptical properties of the ocean, including downwelling irradiance, *Chl*, light backscaterring and others on regular basis and with exceptionally high vertical resolution. These data allowed to make several important insights on the phytoplankton dynamics in different areas of the World Ocean (see reference list in (http://biogeochemical-argo.org/).

In 2014-2015 several Bio-Argo floats were released in the Black Sea. The measurements of these Bio-Argo recently were used to study processes on the oxic-anoxic interface, oxygen variability, particle distribution and diapycnal mixing in the Black Sea (Stanev et al., 2013, 2017, 2018; Capet et al., 2016). In (Kubryakova et al., 2018) seasonal dynamics of depth-averaged *Chl* were estimated on the base of Bio-Argo data. In (Kubryakov et al., 2019a) the response of the vertical distribution of *Chl* on several storms was described. Patterns of the seasonal and interannual variability of vertical distribution of *Chl* were briefly discussed in (Kubryakov, Stanichny, 2016; Stanev et al. 2017) and the relation of *Chl* and light attenuation at 490 nm was obtained in Organelli et al., 2017. (Callieri et al., 2019) use this data to investigate the phenomena of “deep red fluorescence” in the basin. In (Kubryakov et al., 2019a) these measurements were used for a detailed study of the vertical evolution of summer and winter coccolithophore blooms in the Black Sea, their relationship with *Chl* variability and the effect on the formation of dissolved organic matter. However, to date, detailed studies of *Chl* variability related to changes in hydrophysical and optical characteristics conducted on a basis of Bio-Argo data were absent.

In this study we use the 5-year (2014-2018) high-resolution Bio-Argo measurements of *Chl* and PAR to investigate the seasonal variability of *Chl* in different years, its relation with light characteristics and other physical factors. In the first part of the paper we consider the seasonal variability of vertical distribution of PAR, its impact on the *Chl*, and the relation between Chl and PAR attenuation. Further, the seasonal succession of *Chl* in the Black Sea is divided on seven different stages: winter minimum, early spring maximum, April-May minimum, two summer subsurface maximums, early autumn decrease of *Chl* and late autumn *Chl* peak. The roles of different abiotic and biotic factors (mixing, cross-shelf transport, grazing) on the development of each of these stages are discussed.

2. Data and methods

The study is based on data of 4 Bio-Argo floats measuring continuously the biooptical characteristics in the Black Sea during 2014-2018 period. Data were downloaded from IFREMER data archive (ftp://ftp.ifremer.fr/). Most of the time the buoys were located over the continental slope or in the deep basin (depth > 1000 m) (fig.1). The vertical resolution of Bio-Argo data was 1 m, the temporal resolution varied from 1 to 5 days.

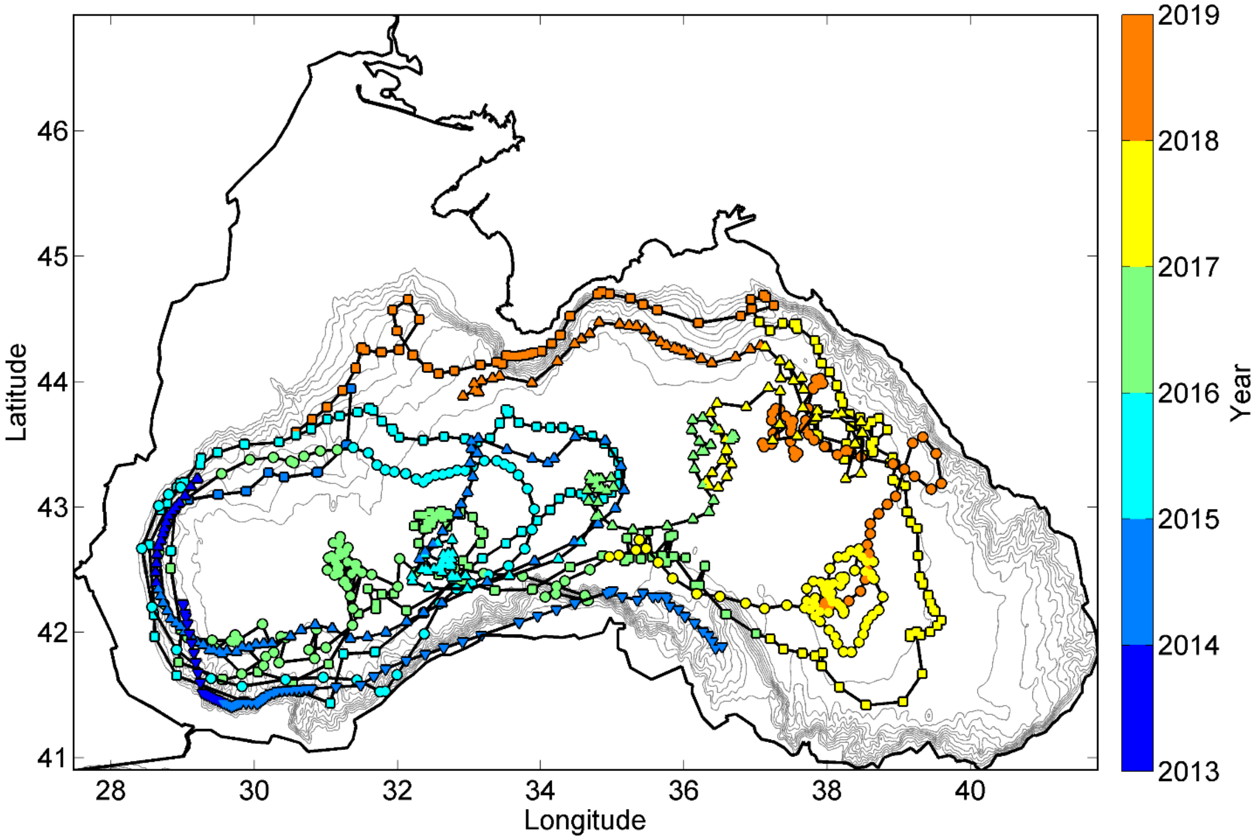

Fig.1 Trajectories of the Bio-Argo floats in January, 2014 – December, 2018 superimposed on the bathymetry contours. Colors show the year of the measurements, markers – different buoys.

Data on the *Chl*, backscattering coefficient at 700 nm (bbp) and downwelling instantaneous irradiance (*Ed*, μmol photons m^{-2} s^{-1}) integrated over 400–700 nm (PAR) were analyzed. *Chl* (mg m^{-3}) was retrieved from the chlorophyll fluorescence sensor of the Wetlabs ECO Triplet Puck using the retrieval equation described by Xing et al. (2011). Measurements of *Chl* were made near the local noon on ascending phase and near the midnight in descending phase of Bio-Argo buoy movements. Thereby these data represent both night and day measurements of fluorescence. Totally more than 1050 profiles of *Chl* were available for 2014-2018 period.

Multispectral ocean color radiometer (OCR-504, SATLANTIC Inc.) was used to measure PAR in the water column (Xing et al., 2012). Most of *Ed* measurements were made near the local noon time on ascending movement of the buoys. In the study we use only *Ed* measurements made within ± 1.5 hours from noon (10:30-13:30 hours). Totally 518 profiles were selected, and 50 were excluded from the analysis. Neglecting daily variations of cloudiness, *Ed* measurements near noon represent approximately the maximal daily downwelling irradiance.

Vertical gradients of *Ed* were used to compute the diffuse attenuation coefficients *Kd(λ):*

$$Kd(\lambda) = \ln\left(\frac{Ed(\lambda, z+dz)}{Ed(\lambda, z)}\right)/dz \qquad (1)$$

here z is depth, dz = 1 m, λ is wavelength.

MODIS-Aqua Level 3 daily data on PAR was obtained from OceanColor data archive (http://oceancolor.gsfc.nasa.gov/). The comparison between the values of the PAR from MODIS sensor and *Ed* measured at 1m depth by underwater color radiometer showed good agreement in values and seasonal variability (Fig. S1 in electronic supplement). Generally, irradiance at 1m depth was 1.4 times lower than that at the surface (see fig. S1b) This difference can be explained by the light attenuation in 0-1 m layer and it is in good accordance with computed values of *Kd* (see table 1).

The rate of photosynthesis primarily depends on the daily integrated solar radiation (*Qs*, mole photons m^{-2} d^{-1}). This value can be estimated from the maximum PAR at noon (*Ed*) and daylength (*DL*), which is a function of latitude *y* and day of a year *nd* (Kirk et al., 1983; Legendre et al., 1993).

$$Qs = 2DL(y, nd) \cdot Ed/\pi \qquad (2)$$

For the Black Sea latitudes (40-45 °N) daylength increases from 9 hours in December to 15 hours in June. At that, the linear slope between *Qs* and *Ed* varies approximately from 5.5 to 9 in winter and summer, respectively.

Argo buoys provide data of salinity and temperature, which were used to compute profiles of potential density at the time of the biooptical measurements. The accuracy of the Argo temperature, salinity and pressure sensors is generally better than 0.002°C, 0.01 and 5 m (Argo Science Team, 2013). The MLD was estimated from Bio-Argo profiles using potential density threshold of 0.07 kg m^{-3} (Kubryakov et al., 2019c).

MODIS-Aqua Level 2 daily data on *Chl* with 1 km spatial resolution were downloaded from OceanColor data archive (http://oceancolor.gsfc.nasa.gov/). *Chl* was calculated using the ocean three-band algorithm for MODIS (OC3M) (O'Reily et al., 1998). Data were routinely corrected on atmospheric and sea surface effects using standard OceanColor atmospheric correction algorithm.

3. Sources of nutrients for the Black Sea phytoplankton

The Black Sea is one of the examples of the very specific marine environment. The basin is almost enclosed, with the only one narrow connection with the rest ocean through the Bosporus strait. The Black Sea is characterized by the very strong haline stratification caused by the large fresh river water inflow in upper layers and salt inflow in the bottom layers from the Mediterranean Sea (see review in Ivanov, Belokopytov, 2013). Strong halocline suppresses vertical mixing in the basin due to which the MLD in the center of the sea usually do not exceed 50 m during its seasonal maximum (Titov, 2004).

The vertical entrainment of the deep remineralized biogenic elements to photic zone is the important source of nutrients for the Black Sea phytoplankton (Sorokin, 1983; Yunev et al., 2002, 2005; Finenko et al., 2005, 2014). The main physical reasons of such entrainment are the winter convection and/or wind turbulent mixing. In the strongly stratified Black Sea the depth of nutricline is associated with certain isopycnals (see e.g. Konovalov et al., 2005). Therefore, during a cold period of a year the density of the upper layer can be used as an indicator of the intensity of the vertical entrainment of nutrients (Kubryakova et al., 2018). Higher density corresponds to higher upward flow of entrained nutrients. The upper part of nutricline in the Black Sea is located approximately below the isopycnal of 1014.2 kg m^{-3} Maximum of nitrate and peak of phosphate concentrations are associated with isopycnals of 1015.5 - 1015.7 kg m^{-3} (Konovalov, Murray, 2001). Seasonal evolution of potential density computed from Argo data showed that maximum density in the upper layer reached 1014.2 kg m^{-3} at $z = 20$ m in February-March, the coldest months (fig. 2a, b). Therefore, in these months, the flow of deep nutrients to the mixed layer is expected to be maximal, which in turn results in the late-winter/early-spring phytoplankton bloom in the Black Sea, as well as in many other areas of the World Ocean. The vertical entrainment of nutrients in the central part of the Black Sea in winter is controlled both by turbulent mixing and upwelling processes. The latter is defined by the intensity of the cyclonic circulation in the sea centre. In February-March cyclonic circulation is maximal bringing the nutricline closer to the surface (isopycnal 1014.2 kg m^{-3}), which is well seen in seasonal density diagram (fig. 2a).

It should be noted that due to strong haline stratification the convectional mixing in the Black Sea does not penetrate below the upper part of pycnocline and the density at the MLD rarely exceeds

1015 kg m^{-3} (Kubryakov et al., 2019c). In the central part of the Black Sea, this density is observed at a depth of 40-50 m, which means that the MLD in winter rarely extends deeper. Lowest MLD are observed in the areas of downwelling, over the continental slope or in mesoscale anticyclones (Ilyin, Belokopytov, 2005; Kubryakov et al., 2019c), where the MLD can reach extreme values for the Black Sea 100-140 m.

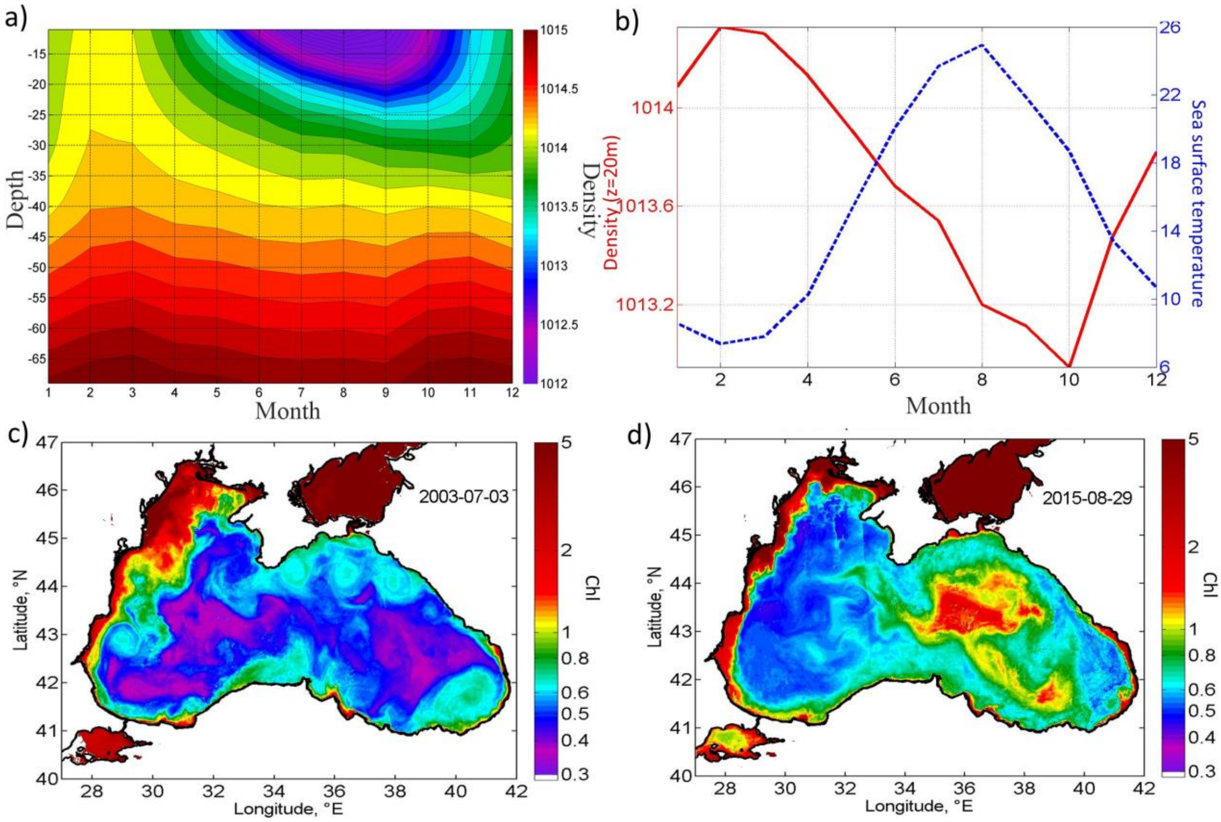

Fig. 2. *a)* Season-depth diagramm of density (kg m^{-3}) computed from Argo floats data; *b)* Seasonal variability of density at z = 20 m and temperature at z = 1 m; *c)* Modis map of *Chl* (mg/m^3) on 3 July 2003 demonstrating impact of mesoscale anticyclones on the cross-shelf transport of *Chl*; *d)* Modis map of *Chl* (mg/m^3) on 29 August 2015 demonstrating anomalous surface bloom in the deep part of the Black Sea caused by the impact of several strong wind events. (see Kubryakov et al., 2019a)

Rivers brings vast amount of dissolved organic matter in the basin (Becquevort et al., 2002), which significantly reduce the water transparency (Vladimirov et al., 1997; Organelli et al., 2017). Shallow MLD, transparency and oxygen deficient make the productivity layer in the Black Sea significantly shallower than in the open areas of the World Ocean. Large river discharge brings vast amount of nitrogen, phosphorus and silicate in organic and inorganic forms to shelf areas of the Black Sea (Cociasu and Popa, 2004). Further, they are transported to the center of the basin upon the action of the mesoscale eddies, upwellings, wind drift currents and other hydrodynamic factors (Yankovsky et al., 2004; Karageorgis et al., 2014; Kubryakov et al., 2018a). Due to relatively small basin area these cross-shelf fluxes plays the important role in the total supply of nutrients to the central Black Sea and functioning of its ecosystem (Oguz et al., 2002; Kubryakov et al., 2016). Cross-shelf transport has a large interannual variability (Kubryakov et al., 2016, 2018b), which is strongly related to the intensity of the large-scale Rim current - dynamic barrier for the shelf particles (Zatsepin et al., 2003; Yankovsky et al., 2004) and the horizontal advection of shelf waters by mesoscale eddies (Zatsepin et al., 2003; Shapiro et al, 2009; Zhou et al., 2014; Kubryakov et al., 2016, 2018a). Mesoscale anticyclones are able to trap nutrient-rich shelf waters in their orbital movement and transport them across the isobaths to the continental slope of the basin (Sur, Ilyin, 1997; Ginzburg et al., 2002; Oguz et al., 2002; Shapiro et al., 2010). An example of such process is shown on the Modis-Aqua map for 3 July 2003 (fig. 2c). On this optical image at least 6 mesoscale anticyclones were located in the north-eastern, south-eastern and western parts of the basin occur. Such anticyclones are characterised by increased *Chl,* as they trap the shelf waters rich in *Chl* and nutrients in their orbital motions. The cross-shelf transport induced by one such large anticyclone can exceed 0.3 Sv (Zhou et al., 2014). Eddy dynamics and cross-shelf transport in the Black Sea intensifies in summer. In this period large-scale Rim current weakens due to decrease of wind curl and breaks down on several large anticyclones (Zatsepin et al., 2002, 2005; Kubryakov, Stanichny, 2015a,b). The seasonal variability of the number of anticyclones in the Black Sea shows that maximum anticyclones are observed in June (Kubryakov, Stanichny, 2015; Kubryakov et al., 2018c). At the same time, they reach a peak of their orbital velocity in September. Therefore, horizontal transport of nutrients is highest in summer-early autumn, on opposite to the vertical transport, which intensifies in winter-early spring. The variability of the eddy dynamics and associated cross-shelf transport is one of the reasons of the interannual changes in the phytoplankton taxonomic composition in the Black Sea in summer (Mikaelyan et al., 2018).

Another mechanism responsible for the vertical entrainment of nutrients is the storm induced mixing. Such events after strong winds were observed in the Black Sea during several years, e.g. in 2001 (McQuatters-Gollop et al., 2008), in 2015 (Kubryakov et al., 2019a) and in 2017 (Zatsepin et al., 2017). Strong wind causes the increase of the MLD and diapycnal mixing in deeper layers driven by shear of intense inertial currents (Kubryakov et al., 2019a). This is accompanied by the local upwelling on the left periphery of wind jets and acceleration of the cyclonic circulation. Mixing over upwelled areas leads to the erosion of nutricline, entrainment of new nutrients to photic layer and sharp increase of the biological productivity. Particularly, in August 2015 several strong wind events lead to the rise of surface MODIS derived *Chl* to 5 mg m^{-3} (fig. 2 d) (Kubryakov et al., 2019a), which is extremely high value for the central Black Sea. Such short-term extreme atmospheric events are one of the triggers for the start of the phytoplankton bloom in autumn (Mikaelyan et al., 2017b).

4. Relation between chlorophyll-a and light conditions

4.1 Dependence of vertical distribution of chlorophyll-a on Photosynthetically Available Radiation

Monthly interannual variability of *Chl* calculated by averaging measurements of all 4 buoys showed that during almost all seasons high values of *Chl* exceeding 0.8 mg m^{-3} were detected in the water column (fig. 3). However, the depth of *Chl* peak significantly varied in time. In autumn-winter high values of *Chl* were located in the upper layers, while in a warm period of a year *Chl* was minimal near the surface. High values of *Chl* in spring-summer were located below the MLD (red line in fig. 3) in the seasonal thermocline or below it.

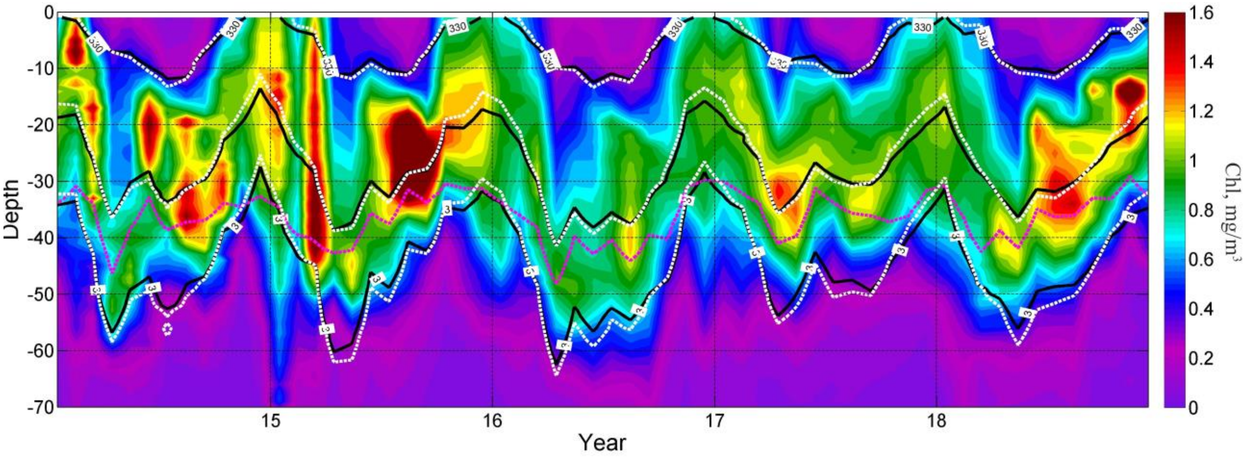

Fig. 3. Monthly variability of the vertical distribution of *Chl* during 2014-2018 from Bio-Argo data. Black lines show isolines of *Ed* = 3, 20 and 330 µmol quanta m^{-2} s^{-1} (from bottom to top), white lines show isolines of *Qs* = 0.08, 0.6 and 10 mol quanta m^{-2} d^{-1} (from bottom to top). Magenta line shows the euphotic layer depth (*Ze*).

To estimate the relation between *Chl* and light conditions, we computed the diagram of dependence of *Chl* on ln(*Ed*) on the basis of all available data in 0-60 m layer (fig. 4a, b). More than 33000 of synchronous measurements of *Ed* and *Chl* were used for this task. In logarithmic coordinates dependence of *Chl* versus ln(*Ed*) has quasigaussian shape (fig. 4b – bottom scale). The dependence *Chl* on ln(*Qs*) has the same shape (fig. 4b – upper scale). *Chl* was minimal under both low and high values of irradiance. Relatively low values of *Chl* (*Chl* < 0.5 mg m^{-3}) was detected at ln(*Ed*) < 1 and ln(*Qs*) < -2.2, which corresponds to *Ed* < 3 µmole photons m^{-2} s^{-1} and *Qs* < 0.08 mole photons m^{-2} d^{-1} (fig. 4b). *Chl* was low at ln(*Ed*) > 5.5 and ln(*Qs*) >2 (*Ed* > 330 µmole photons m^{-2} s^{-1} and *Qs* > 10 mole photons m^{-2} d^{-1}). Below and above these thresholds most *Chl* measurements give low values (fig. 4a). Relatively high values of *Chl* above 0.8 mg m^{-3} were observed under moderate light conditions (*Ed* from 8 to 100 µmole photons m^{-2} s^{-1} and *Qs* from 0.15 to 3 mole photons m^{-2} d^{-1}) and maximum values correspond to *Ed* = 20 µmole photons m^{-2} s^{-1} and *Qs* = 0.6 mole photons m^{-2} d^{-1}.

The dependence *Chl* on *Ed* can be approximated as gaussian function:

$$Chl = a * \mathrm{e}^{\frac{-(\ln(Ed)-\mathrm{b})^2}{c}} + d = 0.97 * \mathrm{e}^{\frac{-(\ln(Ed)-3.13)^2}{2.5}} + 0.06 = 0.94 * \mathrm{e}^{\frac{-(\ln(Qs)+0.46)^2}{2.42}} + 0.11 \quad (3)$$

Here constant *d* = 0.07 defines lowest values of *Chl* detected by Bio-Ago which was non-zero even in very deep layers (500 m). The substantial deep fluorescence is a feature of the Black Sea deep waters, which is considered to be related to the inaccuracy of measurements or “deep red fluorescence” caused by high concentration of organic matter (Callieri et al., 2019)

Constant *a* = 0.97 defines the average amplitude of the *Chl* variability which changed from *d* = 0.07 to 1.04 under different light conditions. Constant *b* = 3.13 defines the position of the maximum of the curve. Therefore, such values of irradiance represent light conditions under which the maximum of *Chl* is observed in the sea. Maximum of *Chl* corresponds to ln(*Ed*) = 3.13 or *Ed* = 22 µmole photons m^{-2} s^{-1} and to ln(*Qs*) = -0.5 or *Qs* = 0.6 mole photons m^{-2} d^{-1}.

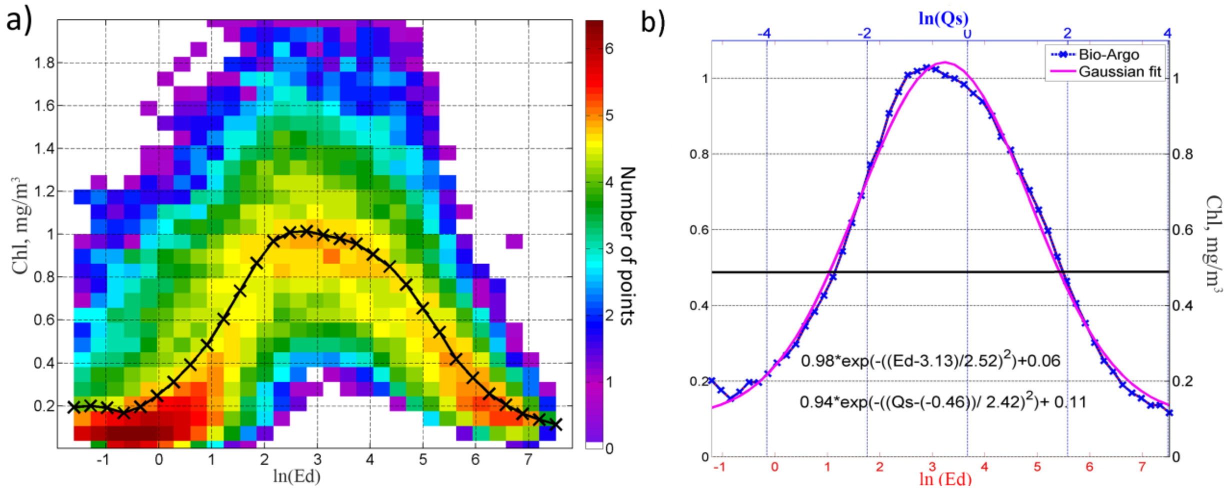

Fig. 4. The dependence diagram between *Chl* and PAR, computed using all available data: a) *Chl* versus ln(*Ed*), where *Ed* is the instantaneous daily PAR (µmole photons m^{-2} s^{-1}) near noon (colors show the number of concurrent measurements, black line shows average numbers); b) averaged dependence of *Chl* on ln(*Ed*) - bottom scale, and on ln(*Qs*) - top scale, where *Qs* is a total daily PAR (mole photons m^{-2} d^{-1}).

Positions of *Ed* and *Qs* isolines varied greatly over time (fig. 3, black and white lines). However, in all seasons *Ed* = 3 µmole photons m^{-2} s^{-1} and *Qs* = 0.08 mole photons m^{-2} d^{-1} restricted the zone of high *Chl* from below, while *Ed* = 330 µmole photons m^{-2} s^{-1} and *Qs* = 10 mole photons m^{-2} d^{-1} coincide with the upper border of the most *Chl* rich layer. The core of the deep *Chl* peak most of the time closely corresponds to depths of isolines *Ed* = 20 µmole photons m^{-2} s^{-1} and *Qs* = 0.6 mole photons m^{-2} d^{-1}. At the same time, positions of these isolines closely corresponded to each other. In winter, when a day is short, isolines of *Qs* = 0.08 mole photons m^{-2} d^{-1}were located on 2-3 m above the isoline *Ed* = 3 µmole photons m^{-2} s^{-1}. In summer, when a day is longer it was located on 2-3 below it. Therefore, these parameters are roughly equal and further we will plot only isolines of *Ed*.

As the nutrient limitation of cell growth is not crucial at the bottom of the photic zone, the light and grazing by zooplankton are the main factors defining phytoplankton vertical distribution. At the same time increased concentration of nutrients and decreased light lead to highest cellular *Chl* in the phytoplankton (Finenko et al., 2003).

Nevertheless the sharp decrease of *Chl* at depths below *Ed* = 3 µmole photons m^{-2} s^{-1} can be a witness of rapid *Chl* deterioration under light conditions insufficient for cell survival. The value of *Qs* = 0.08 mole photons m^{-2} d^{-1} is in agreement with the in-situ estimates of the compensation irradiance (Marra, 2004) (0.06-0.3 mole photons m^{-2} day^{-1}) in the North Atlantic, but it is significantly lower than 1.24 mole photons m^{-2} day^{-1} estimated from satellite data in the same region (Siegel et al., 2002). The obtained value also is slightly lower than 0.415 mole photons m^{-2} day^{-1} used in several recent Bio-Argo studies (Boss and Behrenfeld, 2010;, Xing et al., 2019). It seems that, at the first approximation, the *Qs* of 0.08 mole photons m^{-2} d^{-1} can be considered as a value close to the compensation irradiance for the Black Sea phytoplankton.

The sharp decrease of *Chl* above *Ed* of 330 µmole photons m^{-2} s^{-1} (fig. 4a) can be related with a set of reasons: low nutrient concentration in the upper layer, high irradiance leading to photoinhibition effect and sharp decrease in cellular *Chl* (see Finenko et al., 2002; Churilova et al., 2017). Another reason of this decrease is the non-photochemical quenching - a response of phytoplankton to high light which results in a reduction of fluorescence per unit chlorophyll (Kiefer, 1973; see details in Bittig et al., 2019). All these factors act in the same direction and it is impossible to separate weight of these factors based on our data on *Chl* dynamics. The similar result of the crucial impact of photoacclimation on *Chl* in the South China Sea was obtained recently in (Xing et al., 2019)

At the same time, maximal *Chl* values observed in the range of *Qs* from 0.15 to 3 mole photons m^{-2} d^{-1} indicate that at these optical depths the phytoplankton cells often find the optimum balance between the light and nutrient concentrations. Instantaneous *Ed* from 8 to 100 µmole photons m^{-2} s^{-1} in this layer are close to range from 16 to 82 µmole photons m^{-2} s^{-1} reported for the DCM in the north-western Mediterranean Sea (Latasa et al., 1992). Such irradiances are lower than saturating level for cell growth (Paasche, 2001), while quite comparable for light half-saturation constants which usually reported for various phytoplankton groups (Buitenhuis et al., 2008, Richardson, 2009; Stelmah, Mansurova, 2012). Generally, the relationship between depth of the *Chl* maximum and certain isolumes (fig. 3, 4) illustrates that variations of downwelling irradiance largely control the vertical position of the phytoplankton deep peak in the Black Sea and can noticeably affect its displacement from season to season.

4.2 Seasonal variability of Photosynthetically Available Radiation

The seasonal-vertical diagram of *Ed* and its variability at 1, 20 and 40 m was computed on the base of Bio-Argo floats # 6901866, 7900591 and 7900592 (fig. 5a, b). Note that *Ed* represents daily maximum of instantaneous PAR near the noon. With the beginning of spring the water column becomes strongly stratified and *Ed* at z = 1 m exceeds 800 µmole photons m^{-2} s^{-1}. It is natural that *Ed* is highest in summer when the sun is in high position. In June-July, just below the sea surface (z = 1 m) it reaches seasonal maximum equal to 1150 µmole photons m^{-2} s^{-1}. In summer isoline *Ed* of 330 µmole photons m^{-2} s^{-1} reaches lowest depth (10 m), which coincides with the average thickness of the summer upper mixed layer (red line on fig. 3). During a day phytoplankton cells trapped within the shallow upper mixed layer are damaged by light. Probably, this leads to the partial photoinhibition of phytoplankton growth (Long et al., 1994; Xing et al., 2019). It may be one of the reasons of the lowest *Chl* observed in the upper mixed layer in summer (fig. 3) which was reported in many studies (Kopelevich et al., 2002; Berseneva et al., 2004; Yunev et al., 2005; Demidov et a., 2008; Krivenko, Parhomenko, 2010; Finenko et al., 2014; Kubryakov et al., 2016). Another and probably more important reason of this minimum is the fast consumption of nutrients after winter, which leads to the seasonal minimum of their concentration in the upper mixed layer. The action of both factors results in strong limitation of phytoplankton growth rate and decreased cellular *Chl* in summer (Finenko et al., 2003, 2005).

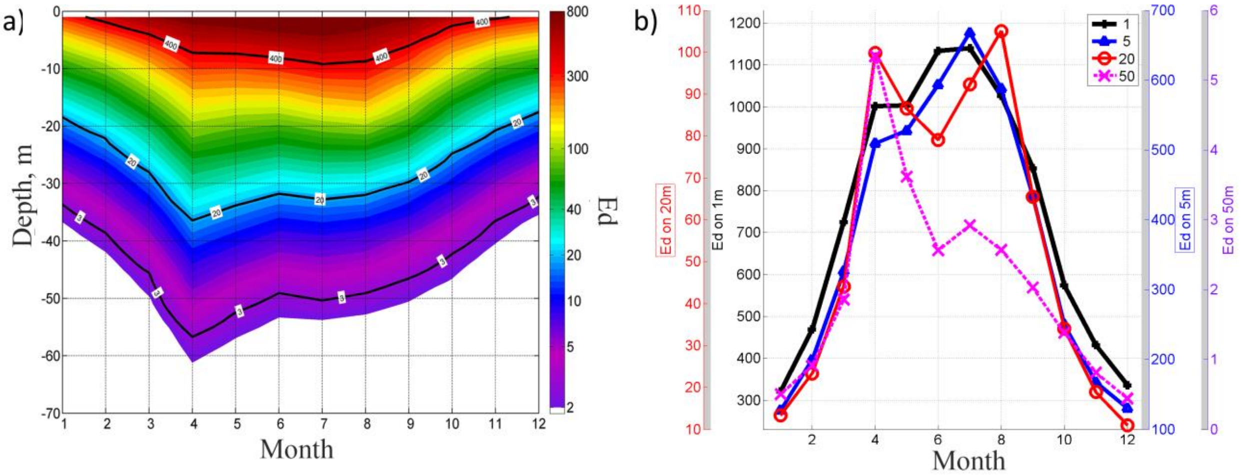

Fig. 5 a) Seasonal-depth diagramm of *Ed (*µmole photons m^{-2} s^{-1}): b) Variability of *Ed* at z = 1 m (black line and scale), 5 m (blue color), 20 m (red color) and 50 m (magenta color).

Minimum of *Ed* at the surface in the Northern Hemisphere is observed in November-January. During these months *Ed* at z = 1 m is lower than 400 µmole photons m^{-2} s^{-1} (fig. 5b) and even in a thin diurnal mixed layer the effect of photoinhibition/ non-photochemical quenching is negligible. Phytoplankton develops in the upper mixed surface layer. Satellite and in-situ data often showed a rapid increase of surface *Chl* in the Black Sea in winter (Kopelevich et al., 2002; Demidov et a., 2008; Finenko et al., 2014; Kubryakov et al., 2016; Kubryakova et al., 2018). At the same time the lower border of the photic layer corresponded to *Ed* = 3 µmole photons m^{-2} s^{-1} is at its shallowest position (35 m).

Seasonal variability of *Ed* at depth differs from that on the surface. Particularly, at 20 m depth the prominent minimum of *Ed* in May-July and two local peaks in April and September occurred. At 50 m depth, sharp maximum of *Ed* was observed in April. In this month the deepest position *Ed* of 3 µmole photons m^{-2} s^{-1} was recorded approximately at 60 m (fig. 5a). These features were related to the seasonal variations of bioptical water properties, particularly light attenuation by *Chl* and other optical constituents (see Section 4.3).

Euphotic layer depth (*Ze*) is determined as the depth at which 1 % of surface PAR penetrates. Note that as the surface PAR is not available, we use data on irradiance at z = 1 m in order to compute *Ze* from Bio-Argo data. Therefore, the computed depth should be somewhat deeper than depth of *Ze* calculated from surface PAR, as *Ed*(z=1m) is less than *Ed*(z=0m). Despite this, *Ze* superimposed on the seasonal variability of *Chl* (fig. 3, magenta line) usually was located above the bottom boundary of the relatively high values of *Chl*, which were often observed below this isoline. At the same time, isoline *Ed* of 3 µmole photons m^{-2} s^{-1} (or *Qs* = 0.08 mole photons m^{-2} d^{-1}) in all seasons correspond well to the bottom boundary of relatively high *Chl* values.

The value *Ze* is relative and depends on water transparency. Therefore it does not take into account the impact of the strong seasonal variability of surface PAR (fig. 5), which can lead to significant errors in defining the depth of productive zone (Banse, 2004). *Ed* at z = 1 m changed from 1200 to 300 µmole photons m^{-2} s^{-1} (fig. 5b). Therefore 1% of this irradiance will be corresponded to *Ed* of 12 and 3 µmole photons m^{-2} s^{-1} in summer and winter, respectively. Photosynthesis efficiency depends on the absolute values of *Ed* (Jassby, Platt, 1976). Phytoplankton is often observed in the layers which are significantly deeper than the depth corresponding to 1% of surface PAR (Letilier et al., 2004; Marra et al., 2014). Therefore, the usage of the value of *Ed* = 3 µmole photons m^{-2} s^{-1} for the definition of the lower border of the productive zone in the Black Sea intuitively is less robust. The zone above *Ed* of 3 µmole photons m^{-2} s^{-1} (*Qs* = 0.08 mole photons m^{-2} d^{-1}) can be considered approximately as the photic layer (PL).

4.3 Relation of *Chl* and light attenuation in the Black Sea

Seasonal changes of light attenuation *Kd* for PAR estimated from *Ed* data using eq. 1 (fig. 6a, Table 1) demonstrate that the variations of *Kd* resemble seasonal variations of *Chl* (fig. 3). This is obvious, as *Chl* is one of the main absorbing agents of light in the ocean (Morel et al., 2007). Maximum of *Kd* was observed below the upper mixed layer in summer (10-35 m) and in the upper layer (0-15 m) in autumn-winter-spring. These peaks coincided well with increased values of *Chl* corresponding to the late summer and early winter phytoplankton blooms. In the warm period of the year (July-September) the transparent waters with the lowest values of *Kd* were located in the surface layer (0-10), where *Chl* was very low. The water column was most transparent in April, when the values of *Kd* in 10-50 m layer was less than 0.12 m^{-1}. This corresponds to the seasonal minimum of *Chl*, which will be discussed in details in Section 5.2.

Table 1. Monthly averaged values of *Kd* in 5 m bins.

Depth, m	Jan	Feb	Mar	Apr	May	Jun	Jul	Aug	Sep	Oct	Nov	Dec
0-5	0,16	0,16	0,15	0,13	0,13	0,13	0,11	0,11	0,12	0,16	0,17	0,17
5-10	0,16	0,17	0,15	0,13	0,14	0,14	0,13	0,11	0,13	0,14	0,17	0,18
10-15	0,14	0,14	0,13	0,11	0,12	0,13	0,13	0,11	0,13	0,14	0,14	0,16
15-20	0,14	0,13	0,13	0,1	0,12	0,14	0,13	0,13	0,13	0,13	0,13	0,14
20-25	0,13	0,12	0,11	0,11	0,13	0,13	0,14	0,15	0,13	0,13	0,13	0,14
25-30	0,12	0,13	0,11	0,1	0,11	0,13	0,13	0,14	0,13	0,12	0,12	0,13
30-35	0,12	0,11	0,11	0,1	0,11	0,12	0,12	0,13	0,13	0,12	0,11	0,11
35-40	0,11	0,11	0,11	0,1	0,1	0,12	0,11	0,12	0,12	0,11	0,1	0,11
40-45	0,09	0,1	0,1	0,1	0,11	0,11	0,11	0,11	0,1	0,09	0,08	0,09
45-50	0,08	0,08	0,09	0,09	0,1	0,1	0,1	0,1	0,09	0,08	0,08	0,07

Colors show different attenuation coefficient (*Kd*, m^{-1}) ranges: lowest (grey); low (green); moderate (yellow) and high (red).

Monthly averaged values of *Kd* in 0-50 m layer varied from 0.07 to 0.18 m^{-1}. However, the range of instant estimates of *Kd* was larger. According to Bio-Argo measurements in the deep part of the Black Sea *Kd* can be from 0.01 to 0.27 m^{-1} (fig. 6b). Since *Chl* is one of the main absorbing agents in the upper layer of the sea (Finenko et al., 2002) a close relationship between *Kd* and *Chl* can be expected. On the basis of all available estimates of *Chl* and *Kd* it was obtained that this dependence can be approximated as *Kd*(Par) = 0.12 * Chl$^{0.19}$. Most of the data (red and yellow colors on fig. 6b) corresponds well to the curve which means that *Chl* largely governs the light availability in the photic zone. However there is a rather significant dispersion of *Kd* values against the average curve. This is due to other optical constituents on the light attenuation, among which dissolved organic matter is one of the most important in the semi-closed Black Sea basin with hogh river discharge (Vladimirov, et al., 1997; Churilova et al., 2009; Mankovsky et al., 2010; Lee et al., 2015).

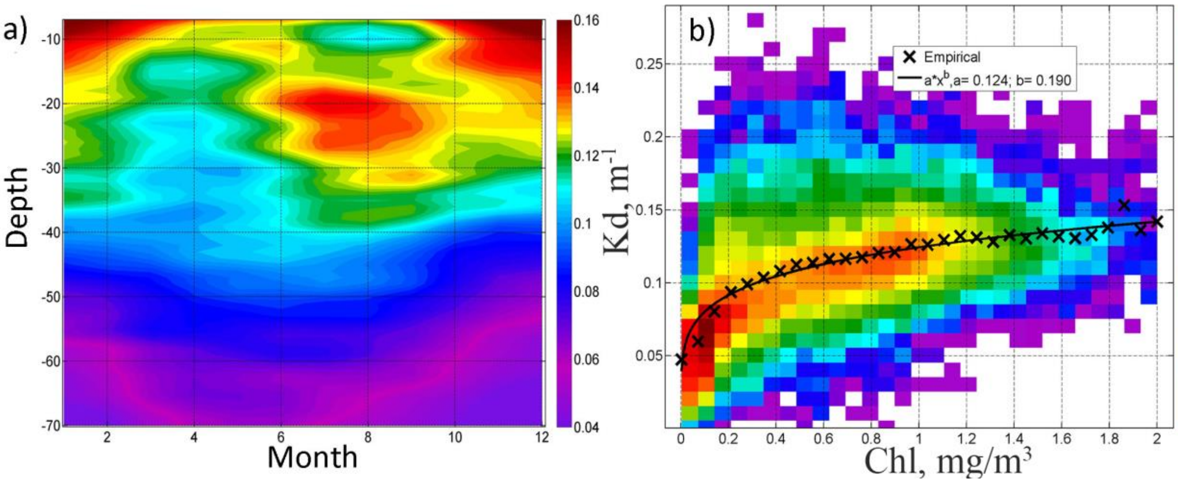

Fig. 6 a) Averaged seasonal-depth diagram of light attenuation coefficient *Kd* (m^{-1}); b) Dependence of *Kd* on *Chl* (mg/m^3) from Bio-Argo data (colors shows number of measurements in a bin).

Particularly, it was shown that in summer the large amount of DOM presumably is released in the subsurface layers of the Back Sea, as a result of phytoplankton cells lysis after the coccolithophore bloom (Kubryakov et al., 2019b). This process, not related directly to the *Chl* dynamics, can strongly contribute to the peak of the light attenuation in subsurface layer (15-25 m) in July-August. Moreover, spectra of absorption of different phytoplankton species differing significantly due to the presence/absence of additional pigments and cell morphology can affect the accuracy of the obtained *Chl-Kd* equation (Mankovsky et al., 2010; Churilova et al., 2008, 2017). Nevertheless, despite these significant issues, we believe that such approximation can be used for rough estimation of *Kd* based of *Chl* data, bearing in mind large statistical amount of the used data.

5. Seasonal stages of chlorophyll-a dynamics

Seasonal diagram of vertical distribution of *Chl* (fig. 7a) averaged over 5 years (2014-2018) shows that throughout a year *Chl* is distributed mainly between isolines of high and low *Ed* (330 and 3 µmole photons m^{-2} s^{-1}) and *Qs* (10 and 0.08 mole photons m^{-2} d^{-1}), respectively. In November-February increased values of *Chl* are observed in the mixed layer (red line on fig. 7a). High *Chl* occurs near the surface. During other months *Chl* maximum is located deeper at depth of 15-50 m. These depths generally correspond to the location of seasonal thermocline and the upper part of the Cold Intermediate Layer (CIL). Deepest position of the *Chl* core (35-50 m) is observed in April. The observed seasonal variability, generally, is in a good agreement with the patterns described in previous studies based on in-situ observations (Vedernikov, Demidov, 1993, 1997; Krivenko, 2010).

The comparison of the depth-averaged *Chl* over 0-60 m depth (blue line on fig. 7b) and surface *Chl* at z = 1 m (red line) shows that their dynamics differ significantly. Depth-averaged *Chl* have three peaks indicating different seasonal blooms in the basin: the first largest peak corresponding to the early spring bloom is observed in March; second peak is observed in August and third peak is detected in November-January in agreement with the previous studies (Vedernikov, Demidov, 1993; Demidov, 1999). The latter peak is the only which occurs on the surface (fig. 7b), that is why only this bloom is well detected via satellite optical measurements (Kopelevich et al., 2002; Kubryakov et al., 2016).

On the basis of the Bio-Argo data the following 7 different seasonal stages of *Chl* dynamics in the Black Sea can be subjectively defined:

1. *February minimum*
2. *March early-spring peak*
3. *April-May depth-averaged minimum and deep peak*
4. *Increased Chl in the thermocline in the second part of May and June*
5. *Subsurface maximum in August*
6. *Early autumn minimum in September-October*
7. *Late autumn-early winter bloom in November-January.*

Chl in the Black Sea is characterized by significant interannual variability (Mikaelyan et al., 1997, Yunev et al., 2002, 2005; Kopelevich et al., 2002; Krivenko, 2010; Kubryakov et al., 2016). Therefore, the calculated average climatic distribution (fig. 7) may noticeably differ from the seasonal dynamics of *Chl* in certain year. However, the analysis of *Chl* in particular years shows that the discussed above stages were manifested more or less clearly in each year of 2014-2018 period (fig. 8). Next we consider these stages one by one.

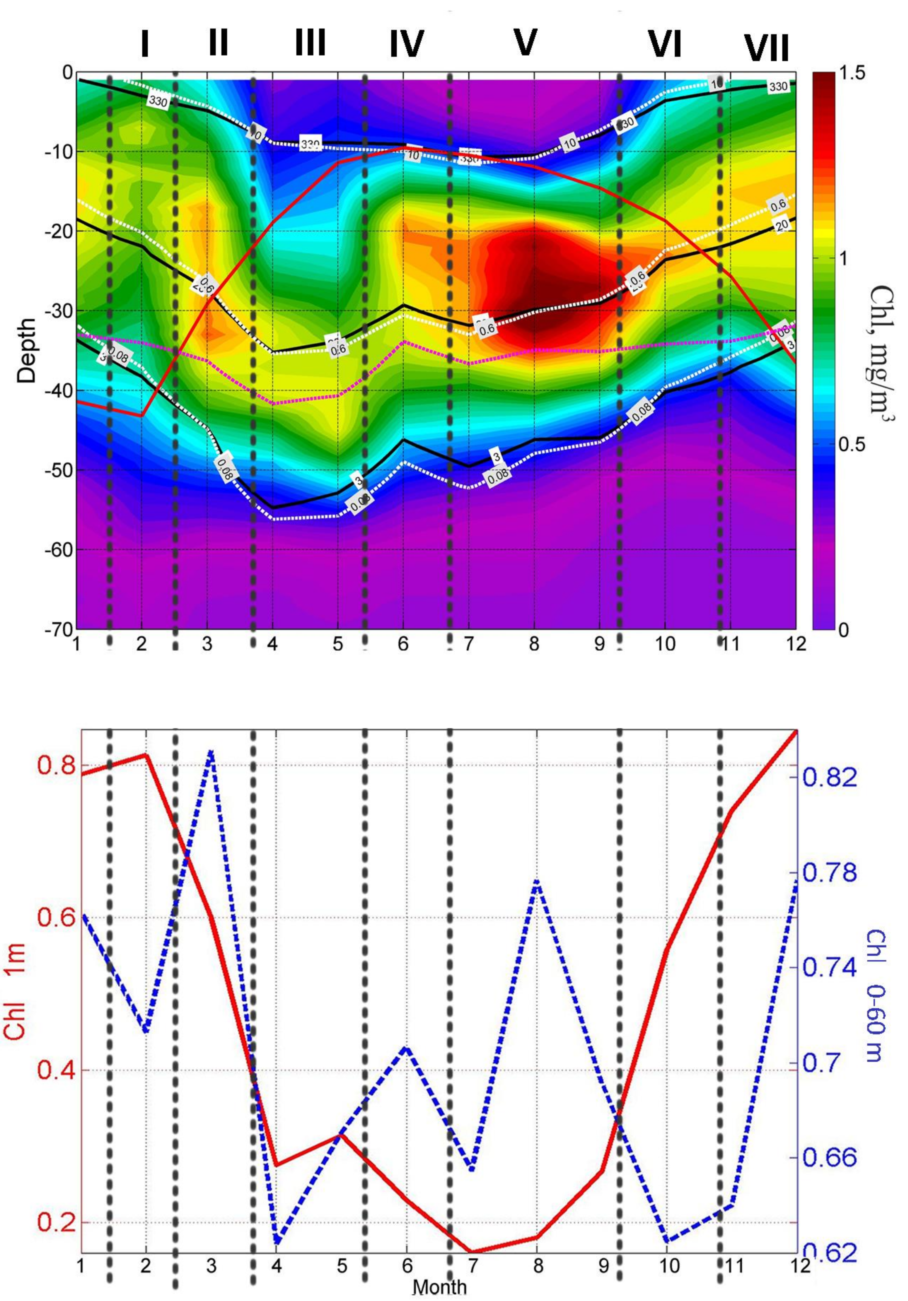

Fig. 7. Multiannual average seasonal variability of the vertical distribution of *Chl* (mg/m^3) in 2014-2018 from Bio-Argo data: a) black (white) lines show isolines of *Ed* (3, 20 and 330 µmole photons m^{-2} s^{-1}) and *Qs* (0.08, 0.6 and 10 mole photons m^{-2} d^{-1}). Red line shows mixed layer depth; b) multiannual average of seasonal variability of column-averaged *Chl* over 0-60 m depth (blue line in fig. 2c) and surface *Chl* at z = 1 m (red line) in 2014-2018. Vertical dash lines separate the different stages of *Chl* dynamics. Roman numbers enumerate the stages.

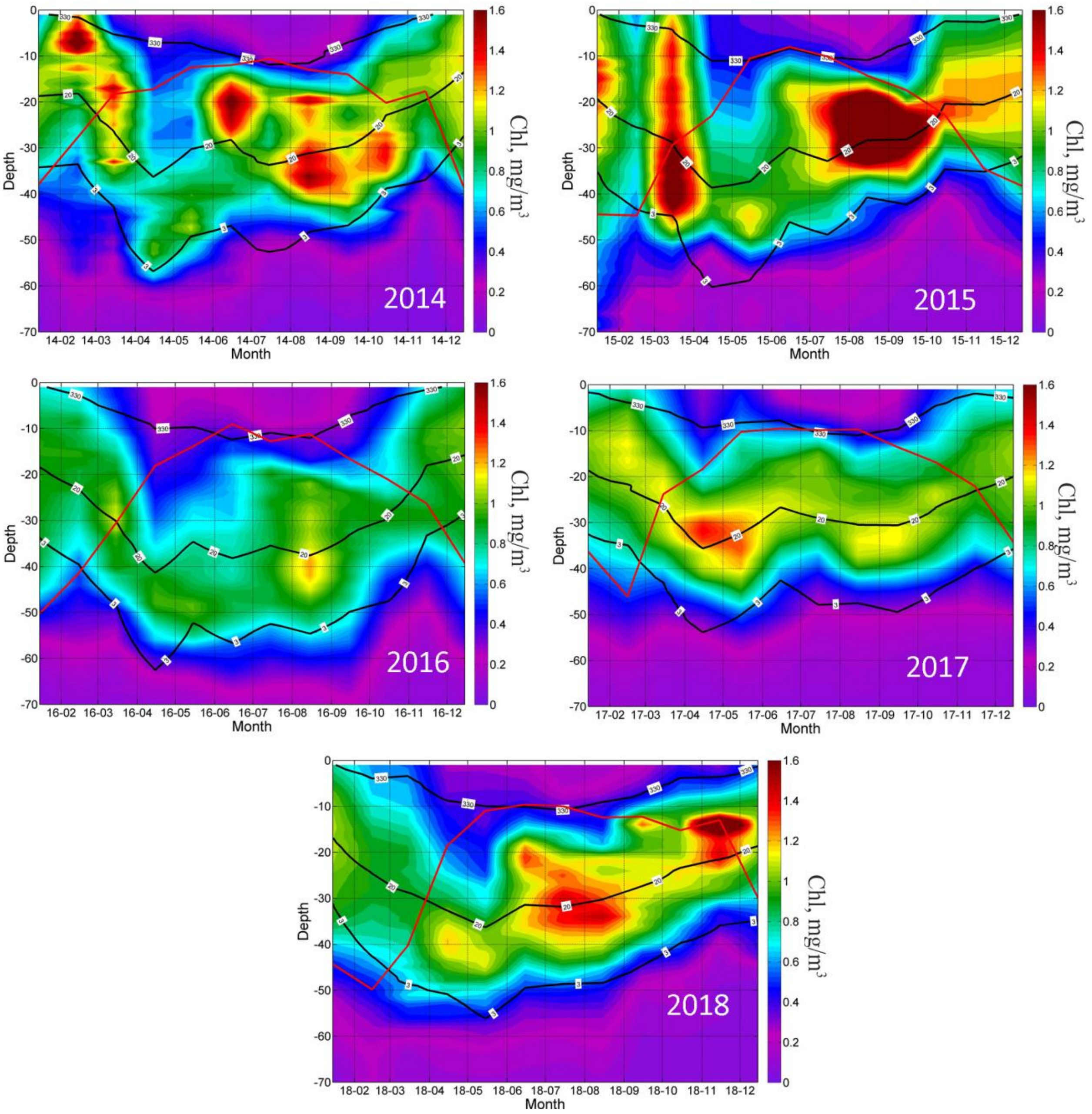

Fig. 8. Vertical diagram of the seasonal dynamics of *Chl* (mg/m^3) in 2014-2018. Black lines show isolumes of *Ed* = 3, 20 and 330 µmole photons m^{-2} s^{-1}. Red line shows the mixed layer depth.

5.1 Stage 1. February *Chl* minimum

During several years (2015, 2016, see fig. 8) a local minimum of depth-averaged *Chl* observed in February reached low values of 0.2 mg/m^3. Illustration of such event was observed by buoy #7900591 in 2016 and 2017 (Fig. 9a). This buoy was floating in the Rim current over the basin continental slope. It is well seen that in both years *Chl* sharply decreased in February in a whole water column and then increased in March. The measured values were less than moderate values of *Chl* (> 0.5 mg/m^3) usually observed in all other seasons. As example, *Chl* profile for 10

February 2016 obtained in the central part of the basin demonstrates that the highest value in the mixed layer did not exceed 0.4 mg/m^3 (fig. 10, I).

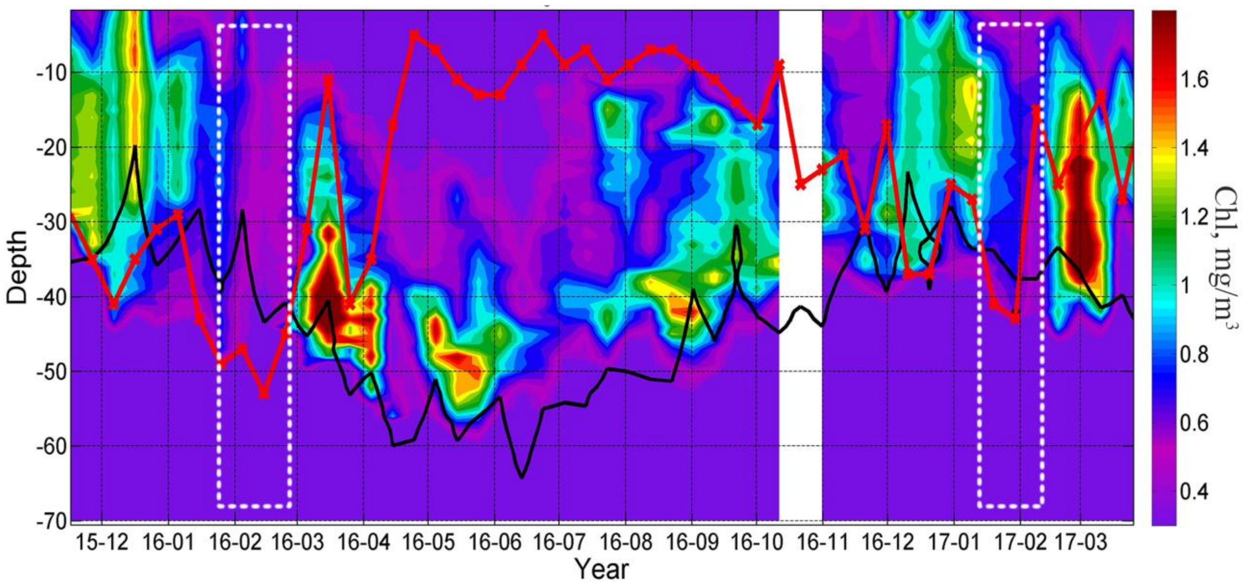

Fig. 9. Detailed vertical variability of *Chl* (mg/m^3) from November 2015 to April 2017 according to the Bio-Argo float #7900591 measurements (time resolution was 1 per 5 days). Black line shows isoline *Ed* = 3 µmole photons m^{-2} s^{-1}. Red line shows the mixed layer depth. White contours show the period of *Chl* minimum.

Comparison of the *Chl*, MLD and *Ed* = 3 µmole photons m^{-2} s^{-1} (corresponding to the lower border of the PL) showed that the sharp decrease of *Chl* in both cases were observed, when the MLD was deeper than the depth of the PL (fig. 9a, red and black lines, respectively). In February 2016 the MLD was 50 m, while the PL was only 35-40 m. In February of 2017 the MLD was 40-45 m, while the PL was 35 m. Therefore, during these periods the phytoplankton cells circulating in the mixed layer were partly locating in darkness, which prohibited their growth. As a result, due to cell mortality or zooplankton grazing amount of phytoplankton decreased. Such effect is well known for open ocean subpolar and boreal areas, where the MLD in winter reaches hundreds of meters, causing winter minimum of *Chl* (Sverdrup, 1953). The same pattern was shown for the Black Sea where the deep mixing prevents phytoplankton growth in winter, which occurs in February firstly during cold winters (Mikaelyan et al., 2017).

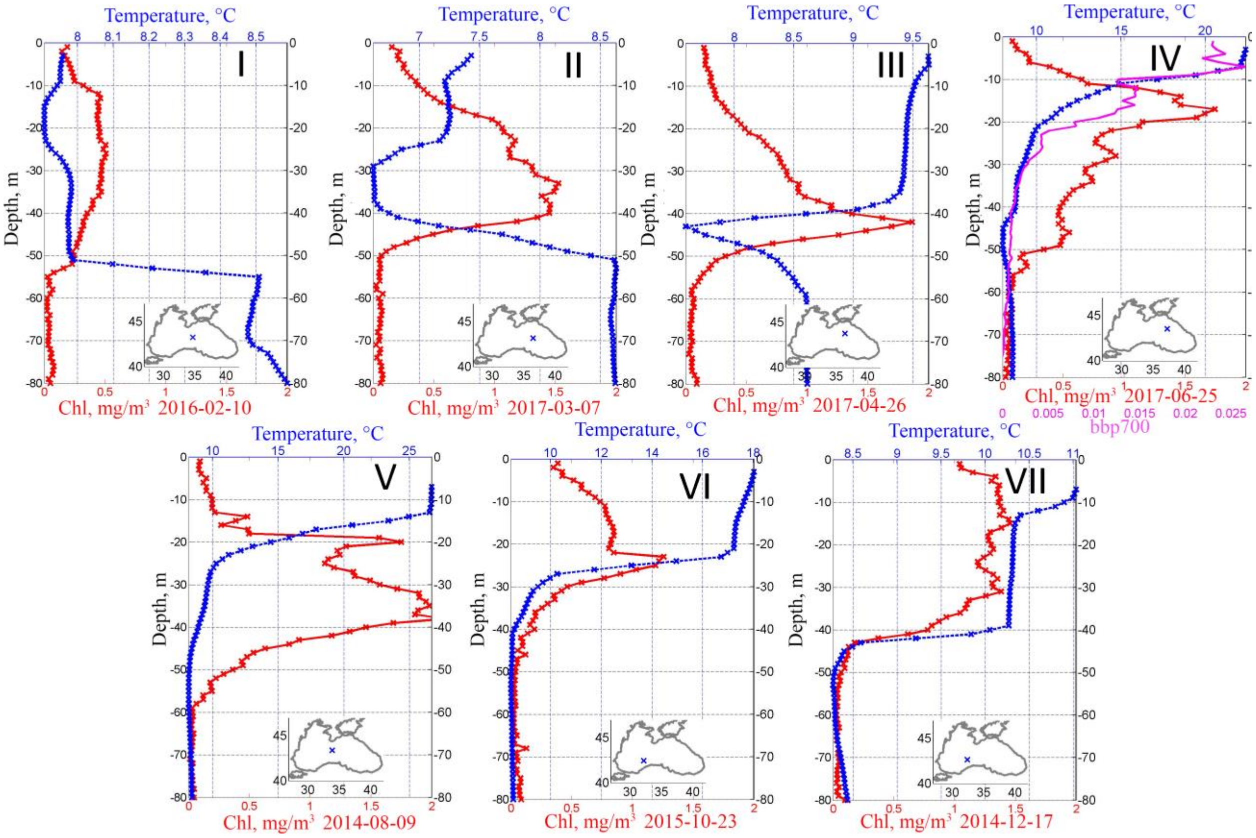

Fig. 10. Examples of typical profiles of *Chl* (mg/m^3 - red color) and temperature (°C - blue color) for each of 7 stages. Magenta line on panel IV shows profile of backscattering coefficient at 700 nm (*bbp*, m^{-1}), reflecting the vertical distribution of the coccolitophore abundance.

Due to strong haline stratification the MLD in the Black Sea is very shallow (Titov, 2004; Kara et al., 2009) as it is restricted by the sharp halocline from below. Prevailing cyclonic circulation uplifts halocline in the basin center and descends it over the continental slope. In the center of the basin the MLD in winter is about 35-40 m depth, whereas on the basin periphery it reaches typically 40-50 m in February (Kubryakov et al., 2019c). At the same time, in mesoscale anticyclones the deepening of pycnocline and convergence of surface waters (Kubryakov et al., 2018b) can lead to the extreme depth of the MLD which reaches 100-150 m inside these structures (Belokopytov, Ilyin, 2010; Kubryakov et al., 2019c).

According to Bio-Argo data the PL in winter is about 35 m (isoline *Ed* = 3 µmole photons m^{-2} s^{-1} on fig. 9a). This is close to the values of the MLD in the center of the Black Sea, but generally is lower than that on the basin periphery. Therefore, it can be expected that the observed February minimum of *Chl* caused by Sverdrup's critical depth effect should be strongest during cold winters over the continental slope of the basin and especially in the mesoscale anticyclones (see also the discussion in Vedernikov, Demidov, 1999; Demidov, 1999). This corresponds to *Chl* dynamics observed in case of the buoy #7900591 (fig. 9), which was situated in the downwelling zone over the continental slope. At the same time this minimum can be less prominent or absent in the sea centre, where strong winter bloom can be observed during very cold years with intense cyclonic circulation, e.g. in 1991 (Krupatkina et al., 1991; Mikaelyan, 1995, Demidov, 1999). Interannual variations of cloudiness also may play partial role in the formation of February minimum by modulation of the amount of incoming PAR at the sea surface. However, the investigation of the relation of PAR and cloudiness are out of scope of this study.

During “mild” winters with low MLD, the February minimum may be absent. In this case, the peak of early spring can begin in February, but not in March, as usual, in the case of a cold winter (fig. 8, 2014). Such impact of winter severity on the timing of the early spring *Chl* peak was recently described in detail (Mikaelyan et al., 2017a). Therefore, climatic-averged *Chl* depends on proportion of warm and cold winters. This can explain the discrepancy of low February *Chl* obtained in our research (0.5 mg/m^3) and high values (1.5 mg/m^3) reported earlier for cold climatic period in the Black Sea region (Finenko et al., 2005). Another reason is the averaging of data from different sea regions, which can differ in conditions of winter cooling. As example, averaging of 4 buoys data did not show a prominent local minimum of *Chl* February (fig. 8, 2016, 2017), whereas the data from one buoy clearly demonstrates this minimum in these years (fig. 9). In addition, usually the duration of this minimum is about 2 weeks, i.e. monthly averaging may overestimate the minimal *Chl* values.

5.2 Stage 2. *March early-spring peak*

The maximal vertical entrainment of nutrients into the upper layers occurs in February-March (see Section 3, fig. 2). However, when the winter is cold and the MLD is deep in February phytoplankton does not develop intensively due to insufficient light. From February to March *Ed* at sea surface rises in two times from 450 to 800 µmole photons m^{-2} s^{-1} (fig. 5). This deepens the PL depth from 40 to 45 m. At the same time the MLD shallows significantly from 45 to 25 m depth due to thermal heating.

Large amount of available nutrients and increased light govern early-spring bloom of phytoplankton, which leads to the highest annual peak of column-averaged *Chl* (fig. 7), described in the number of previous studies (e.g. Sorokin, 1983; Vedernikov, Demidov, 1993; Vinogradov et al., 1999; Finenko et al., 2005). Field investigations showed that this maximum formed mainly by small diatoms which are more competitive in the conditions of high nutrients (Silkin et al., 2019; Mikaelyan et al., 2018).

After the formation of the seasonal thermocline in March, the intense vertical entrainment of nutrients is over. Nutrients in the upper mixed layer are often depleted due to diatom bloom in previous months (Mikaelyan et al., 2017). Besides, PAR at the surface is already too high (> 800 µmole photons m^{-2} s^{-1}) during daytime. This probably results in photoinhibition of the phytoplankton growth, especially in the diurnal thermocline layer occupying upper several meters. As a result, surface *Chl* rapidly decreases in March, which was observed both on Bio-Argo (fig. 7b) and earlier on satellite data (Finenko et al., 2014; Kubryakov et al., 2016).

At the same time, nutrients in high amount exist in the thermocline layer and below it. Under favourable light conditions this causes the rapid development of phytoplankton both in the lower part of the mixed layer and mainly in stratified layers below it (fig. 8, 2014, 2015; fig. 9; fig. 10, panel II).

Rise of *Chl* in early-spring was observed in a water column between *Ed* of 3 and 330 µmole photons m^{-2} s^{-1}, i.e. in the layers with quite favourable light conditions (fig. 7, 8). This is also well seen on profile for 7 March 2017 (fig. 10, panel II). *Chl* was higher than 1 mg/m^3 in 15-45 m layer, but was lower than 0.5 mg/m^3 at 0-10 m. This extended in depth phytoplankton growth results in the highest annual depth integrated *Chl* in March. However, the satellite scanners cannot detect this highest annual early-spring peak of phytoplankton in the Black Sea, as it is mostly located under the mixed layer (Kubryakova et al., 2018).

Usually, the spring phytoplankton bloom in the upper mixed layer is highest during a year in the most boreal and temporal regions of the World Ocean. In the Black Sea, due to regular winter development of phytoplankton in surface layers and depletion of nutrients, this spring bloom develops in the deep layers (fig. 7), which is manifested in the annual *Chl* maximum in this period.

5.3 Stage 3. April-May depth-averaged minimum and deep *Chl* peak

March peak is followed by the sharp decrease of depth-averaged *Chl* with the lowest values in its seasonal dynamics (fig. 7b). In the upper 10-40 m layer *Chl* values fall down twofold from average values of 1 mg/m^3 in March to 0.4-0.5 mg/m^3 in April - first part of May. One of the possible reasons of this decrease is the local seasonal maximum of micro and mesozooplankton in spring (Senicheva, 1979; Shumakova, 1979; Kovalev et al., 2003), which leads to the fast consumption of diatoms after early-spring bloom. The second reason is the depletion of nutrients in the PL due to their consumption by phytoplankton during previous bloom (Sorokin, 1983).

At the same time, in April *Chl* rises significantly at depth of 40-55 m which leads to the seasonal peak in this layer. This is the only period of the year, where *Chl* at 50 m reaches 0.7-0.8 mg/m^3, while in other seasons it is less than 0.5 mg/m^3 (fig. 7, 8). Particularly, in the given example *Chl* at 45 m exceeds 1.5 mg/m^3 (fig. 10, III). This peak corresponds to the position of the minimal temperature in the Cold Intermediate Layer. Similar deep rise of *Chl* in spring was described on the base of in-situ data (Finenko et al., 2005; Krivenko, 2010). Partly, this deep phytoplankton accumulation may be caused by the sinking of spring bloom, which can be observed in Bio-Argo data (fig. 8). Another and probably main reason of increase of *Chl* at this depth is the deepest light penetration in April-May (fig. 5a). The margin of the PL (*Ed* = 3 μmole photons m^{-2} s^{-1}) on average is located at z = 60 m in this time period (fig. 7a).

Such deep light penetration is the result of the minimum light attenuation in April (fig. 6a). It, in its turn, is caused by the seasonal minimum of *Chl* in the upper layers. Therefore, absence of the self-shading by *Chl* leads to the deepest penetration of irradiance. As a result irradiance at 45-60 m is sufficient for the survival and growth of the phytoplankton. At these depths there are high amount of nutrients, which was not consumed during winter-spring bloom, as they were located previously in aphotic zone. Large amount of nutrients and light availability induce phytoplankton bloom at these deep layers. Recent taxonomic analysis showed that the April phytoplankton bloom is mostly formed by dinoflagellates (Mikaelyan et al., 2018). The April phytoplankton bloom was moderate in 2014, 2015 and 2018 (fig. 8a). In relatively warm 2016, the April phytoplankton bloom was almost absent, but it was strong in other years. On contrast, in cold 2017 with strong vertical flow of nutrients in winter, the April deep *Chl* was the highest and its magnitude significantly exceeded the February-March peak. The factors controlling the interannual variability of this bloom is not clear and its relation with winter severity is not quite evident.

5.4 Stage 4. Increased *Chl* in the thermocline in the second part of May and June

After the minimum in April *Chl* began to rise from May to August mainly in the seasonal thermocline and beneath (10-40 m layer) (fig. 8). Two distinct local maxima of *Chl* can be detected in summer period (fig. 7, 8). First smaller peak clearly visible in the graph of seasonal variability of column-averaged *Chl* is observed in June in a very thin layer of 15-20 m. This June thermocline peak was also documented previously (Finenko et al., 2005).

June maximum was especially prominent in 2014 (fig. 8a). During this year it was observed at depth 15- 30 m and was characterized by *Chl* values exceeding 1.5 mg/m^3. The peak was also rather high in 2015 and 2017 (fig. 8b, d), when the *Chl* values were about of 1.2 mg/m^3. In 2017 this local maximum was located in the sub-thermocline layer and was observed both in June and July. On contrast, in 2016 it was absent.

From April to August *Ed* in the near surface layer z = 5 m exceeds 500 μmole photons m^{-2} s^{-1} (fig. 5b). In the mixed layer (0-10 m) low nitrate concentration and high solar radiation restrict the phytoplankton growth in the upper layer (Vedernikov, Demidov, 1997) and result in low *Chl*. In such extreme conditions calcified phytoplankton (coccolithophores) develops in the upper layers of the Black Sea (Pautova et al., 2007; Mikaelyan et al., 2011). Coccoliths defend cells from high insolation, which give them an advantage to develop (Tyrell, Merico, 2004). One of the most powerful coccolithophore blooms in the World Ocean is observed in the Black Sea in May-June, and it is referred as "early summer" bloom (Cokacar et al., 2001; Mikaelyan et al., 2005). Usually, coccolithophores and associated coccoliths occupy the upper 0-15 m layer (Mikaelyan et al., 2005) in the beginning of their blooming and further sinks to deeper layers (Kubryakov et al., 2019b).

June small local peak of *Chl* is observed at the same period as the early summer coccolithophore bloom, but in deeper layers. Of particular interest is very small vertical scale of this peak. The highest *Chl* values usually occupies very thin layer with thickness of about 5 meter (15-20 m). As an example, on 25 May 2017 (fig. 10, panel IV) the profiles of *Chl* and backscattering coefficient at 700 nm (bbp) are shown. It is seen that the relatively large peak of *Chl*, exceeding 1.5 mg/m^3 is observed at the lower part of the surface bbp peak at 0-10 m, which in this period is largely defined by the scattering of the coccoliths. Therefore, non-calcified phytoplankton containing relatively higher cellular *Chl* is located in the lower part of the zone of coccolithophores development. Moreover, interannual variations of the intensity of this *Chl* peak positively correlates with the interannual variability of the intensity of coccolithophore bloom in in 2014-2017. On the basis of the Bio-Argo and satellite data it was shown that the stronger coccolithophore blooms were observed in 2014 and 2017 (Kubryakov et al., 2019b). The high *Chl* peak in the thermocline was also observed during the same years (fig. 8a, d). The coincidence in timing and intensity of June *Chl* peak and coccolithophores bloom evidences that these events may be related.

Several researches detected simultaneous development of coccolithophores and other species of phytoplankton in this period of a year. Particularly, the blooms of diatoms *Chaetoceros subtilis var. abnormis f. simplex* (Pautova et al., 2007) and *Proboscia alata* (Mikaelyan et al., 2018; Silkin et al., 2018) were observed in May-June in the Black Sea together with coccolithophore development. Moreover, it was shown that coccolithophores and diatoms often alternatively develop during this period (Mikaelyan et. al, 2015). High concentration of the small dinoflagellates in May-June was observed in the south Black Sea (Eker et al., 2003). All of these species can contribute to this shallow and thin subsurface *Chl* peak in June.

5.5 Stage 5. Large subsurface *Chl* peak in August

One of the prominent features of *Chl* annual dynamics is extended deep maximum which develops in July-September in the seasonal thermocline and below in 15-40 m layer. This peak is well-known in the Black Sea (Sorokin, 1983; Vedernikov, Demidov, 1997; Finenko et al., 2005) as well as in many other regions of World Ocean (see review in Cullen, 2015).

The rise of summer *Chl* due to growth of phytoplankton can be caused by at least two physical factors (see Section 3): intensification of the cross-shelf transport of nutrients by mesoscale eddies in summer period (Kubryakov, Stanichny, 2015a; Kubryakov et al., 2018a), vertical flux of nutrients due to the nitrocline erosion after strong wind bursts.

On 5-year averaged diagram this maximum was observed in 20-40 m layer from August to September and reached values about of 1.5 mg/m^3 (fig. 8). However, the inspection of the interannual variability of this maximum showed that dominant contribution to this maximum was related to the very high *Chl* values in 2015. These anomalous August phytoplankton bloom was related to the four strong wind events in August 2015, which caused local Ekman upwelling in the deep part of the basin and entrainment of nutrients to the PL (Kubryakov et al., 2019a). This led to the extreme surface *Chl* values > 5 mg/m^3 detected by MODIS in the central Black Sea, for the first time in satellite era, while Bio-Argo buoy recorded peak of 8 mg/m^3 at the lower boundary of the PL (Kubryakov et al., 2019a). These values of the deep *Chl* in 2015 were higher than those reported in previous studies (0.6-1.0 mg/m^3) for summer (Finenko et al., 2005).

In 2015 the August phytoplankton bloom was observed in 15-35 m layer. This is shallower than in other years, which probably was the result of storm-induced upwelling. In other years the August peak of *Chl* was observed deeper (fig. 8). In 2014 and 2017 it was located at depth of 30-40 m, while in 2016 it was observed at 40-50 m. In 2016 August *Chl* peak was lowest (1.1 mg/m^3), in 2014 it was strong (1.4 mg/m^3), and in 2017 it was moderate (1.2 mg/m^3). Often this maximum has bimodal structure with two peaks (see e.g. Finenko et al., 2005; Krivenko, 2010). Similar patterns were often observed in our research. For example, on 9 August 2014 *Chl* exceeded 1.5 mg/m^3 in a very narrow layer (18-20 m) just below the seasonal thermocline and deeper in a wider layer at 30-40 m (fig. 10, panel V).

It should be noted that the increase in *Chl* in the subsurface layers in summer usually does not fully reflect changes in the phytoplankton biomass (Finenko et al., 2002, 2005; Krivenko, 2010; Krivenko, Parhomenko, 2010; Churilova et al., 2017). During this period the peak of the phytoplankton biomass is usually located above the maximum of *Chl* (Finenko et al., 2005; Stelmah, Babich, 2006; Krivenko, 2010). Several studies explained this discrepancy by the photoadaptive response of phytoplankton: the increase the amount of *Chl* in a cell at depth during low insolation and high nutrient concentrations (Finenko et al., 2002, 2005; Churilova et al., 2017). Similarly, photoadaptive response to high irradiance and low nutrients leads to decrease of cellular *Chl* in the upper layers. As a result, deep *Chl* maximum does not correspond to peak in phytoplankton biomass. Moreover, in the Black Sea, the deepest phytoplankton in summer mainly consists of small flagellates and unicellular cyanobacteria (Rat'kova, 1989; Churilova et al., 2018) which have very high specific cellular pigment content. As a result the biomass may be low, whereas the *Chl* is rather high.

In August phytoplankton is often dominated by large diatom *Pseudosolenia calcar-avis* in the upper layers and small colonial *Pseudo-nitzschia pseudodelicatissima* in the thermocline (Pautova et al., 2007; Mikaelyan et al., 2018) or small dinoflagellates (Eker et al., 2003; Mikaelyan et al., 2018). The year-to-year changes of the phytoplankton composition in summer were recently explained by the changes of the dynamic forcing (Mikaelyan et al., 2018). In cold years, which are usually characterized by strong cyclonic winds over the basin, the eddy formation and transport is dampened in summer (Kubryakov, Stanichny, 2015a). In warm years eddy dynamics is more intense and mesoscale anticyclones can bring more nutrients to the deep basin, which favours the development of large diatoms. On contrast, in cold year with reduced cross-shelf water exchange small dinoflagellates have advantage to develop. The obtained results generally are in line with this pattern. After warm winters in 2014, 2015 and 2018 the strong August *Chl* maximum was observed (fig. 8 a, b, e). After cold winter 2017 it was much less pronounced.

Another discussed reason of the August DCM is the recycling of the nutrients after the strong early-summer coccolithophore bloom. Field studies (Mikaelyan et al., 2015, 2018) and model results (Kubryakova et al., 2018) showed that intense vertical entrainment of nutrients during cold winter significantly increase the strength of early summer coccolithophore bloom. The termination of this bloom results in large amount of dissolved organic matter (Kubryakov et al., 2019b), thereby leading to the transfer of trophic energy to the mixotrophic and heterotrophic species through microbial loop (Azam al., 1983). In this way, after cold years with high coccolithophore blooms species with low *Chl* and capability of mixotrophy can develop. Both this factor and low cross-shelf water exchange can explain the lower *Chl* in cold 2017, when the strong coccolithophore bloom occurred, in comparison to 2015 and 2016 with the higher August DCM after weak coccolithophore bloom (fig. 8). It is worth nothing that all possible mechanisms – wind forcing, eddy advection, amount of nutrients entrained in winter, recycling after coccolithophore bloom and others work together or alternatively to cause interannual variations of the summer DCM. The contribution of these processes can vary from year to year depending on meteorological and dynamic conditions.

5.6 Stage 6. Early autumn minimum in September-October

From August to October the column-averaged *Chl* began to decrease (fig. 7b), which is in agreement with field data (Silkin et al., 2018). The minimum column-averaged *Chl* is observed in September-October. One of the probable reasons of this reduction is the active consumption of summer population of phytoplankton. The highest second seasonal peak of zooplankton abundance represented mainly by microzooplankthon is observed in September-October (Kovalev et al., 2003; Stelmah et al., 2013) following the August DCM.

In this period of a year *Chl* rapidly declines in deep layers below 35 m. At these depths, it can decreases 3 times below 0.5 mg/m^3 comparing to summer values (fig. 10, panel VI). At the same time, *Chl* at the surface began to rise (fig. 7, 8). Cooling and rise of wind velocity increase the MLD in autumn from 10 m in August to 20-25 m in October. Nutrients and phytoplankton from the thermocline maximum is entrained to the expanding mixed layer. This leads to the continuous increase of *Chl* in the upper layers and its simultaneous decrease at 10-25 m layer. Therefore, the rise of *Chl* in early autumn at the surface, detected in satellite data (Kopelevich et al., 2002; Demidov et a., 2008; Finenko et al., 2014; Kubryakov et al., 2016; Kubryakova et al., 2018) can be, at least partly, attributed to the vertical redistribution of *Chl*. The same mechanism of surface *Chl* increase in surface layer in autumn was noted in the South China Sea in the recent study by (Xing et., 2019).

5.7 Stage 7. Late autumn-early winter bloom in November-January

In November-December the surface cooling continues to deepen the mixed layer. This is accompanied by the uplift of the nitrocline due to the acceleration of the basin cyclonic circulation in winter (fig. 2a). Strong autumn winds lead to additional erosion of the thermocline and entrainment of new nutrients in to the PL. In early November, the MLD reaches 25 m and its density reaches values close to density of the upper nitrocline layers. Periodic storms lead to injection of nutrients into the mixed layer, which induces the late autumn phytoplankton bloom (Mikaelyan et al., 2017b).

In December-January, the MLD reaches 35-40 m and its density increases to 1014 kg/m^3 (fig. 2b), corresponding to the density of the upper part of nitrocline. This results in the high intense flow of nutrients to the upper mixed layer and causes peak of column-averaged *Chl* in December (fig.7).

Low sun position results in the relatively small average values of *Ed* 300-350 µmole photons m^{-2} s^{-1} at the surface in November-January, due to which the effect of cell growth photoinhibition is minimal. In December the high surface *Chl* (fig. 7b) is detected (0.8 mg/m^3) both by satellite and in-situ data (Berseneva et al., 2004; Demidov 2008; Kopelevich et al., 2002; Nezlin, 2008; Finenko et al., 2014; Kubryakov et al., 2016). *Chl* is slightly lower in the surface layer (0-5 m) than in the layer below (15-20 m) (fig. 7a). As an example, on 17 December 2014 *Chl* was almost uniform (1.4 mg/m^3) in 5-35 m depth in agreement with temperature distribution (fig. 10, panel VII). Increased temperature at the surface is a probable result of diurnal heating, which formed the shallow thermocline in 0-10 m. In the upper part of this thin diurnal layer (0-5 m) *Chl* values were lower (about 1.1 mg/m^3), probably as a result of a decrease of cellular *Chl* or non-photochemical quenching.

At the beginning of January the whole thick mixed layer (0-40 m) was characterized by the high *Chl* of 0.9-1.2 mg/m^3 (fig. 7). As a result the local maximum of column-averaged *Chl* in January was comparable to August peak (fig. 7b). At the end of January the MLD reaches the lower border of the PL. Low average irradiance in the thick mixed layer limits the growth of phytoplankton. However, phytoplankton develops during the periods of calm weather in the temporal shallow upper mixed layer with sufficient light conditions (Mikaelyan et al., 2017a). In February with further deepening of the mixed layer and correspondent decrease in average irradiance the local *Chl* minimum (Stage I) is observed again.

6. Conclusions

Bio-Argo floats provided continuous, simultaneous measurements of several biooptical and physical properties of the Black Sea marine environment. Data available for more than 5 years gave a comprehensive picture of the seasonal evolution of *Chl*, its year-to-year variability and dependence on light conditions. Particularly, it was shown that the vertical distribution of *Chl* in the Black Sea has a clear relation with the daily PAR and can be described by quasi-gaussian dependence. *Chl* was mainly located at depths with a maximum instantaneous PAR (*Ed*) ranged from 3 to 330 μmole photons m^{-2} s^{-1}. The first value represents the approximate optical depth of compensation irradiance for the Black Sea phytoplankton, while the second – level of irradiance above which the photoinhibition/cell photoadaptation or non-photochemical quenching lead to decrease of estimated *Chl*.

From March to October *Ed* exceeds 330 μmole photons m^{-2} s^{-1} in the upper layer of 10-20 m, where the *Chl* is low. Maximal values of *Chl* were observed near isoline *Ed* of 20 μmole photons m^{-2} s^{-1} (daily integrated irradiance Qs = 0.6 mole photons m^{-2} d^{-1}). Such illumination is often observed at depths, where, apparently, for the growth of phytoplankton, an optimal balance is achieved between the light conditions and the concentration of nutrients. The seasonal variability of these isolines largely controls the vertical position of the *Chl*-rich layer throughout all seasons of the year.

On the other hand, *Chl* in its turn also governs the depth of the photic layer, as its variations largely affect seasonal variability of light attenuation. The relation of *Kd* with *Chl* is parameterized by the power function. The highest averaged *Kd* in the upper 30-m layer observed in October-March were 0.15-0.17 m^{-1}, in July-September 0.13-0.15 m^{-1}. The water column was the most transparent in April (0.1-0.13 m^{-1}), when *Chl* was in its sharp annual minimum.

One of the significant differences between the Black Sea and the open ocean areas of the same latitudes is the strong haline stratification, which leads to low mixed layer depth. Due to this almost in all period of a year the mixed layer in the center of the basin is situated above the bottom boundary of photic layer. The exception is February, when during cold years, especially in the areas of downwelling, the mixed layer can exceed 40-50 m, which is below the compensation depth, located at these time approximately at 35-40 m. The Sverdrup’s effect in this case causes sharp decrease of *Chl* in the upper layer in February.

In March rise of the downwelling irradiance, formation of seasonal thermocline and sufficient nutrients vertically entrained from deeper layers in winter governs the growth of phytoplankton. This leads to the sharp increase of *Chl* observed both in the lower part of the mixed layer and in seasonal thermocline.

The deepest position of the photic layer in the Black Sea is observed in April, when the waters are cleanest and *Kd* is minimal through all water column. The low light attenuation in upper layers allows light penetrating to the maximum depth up to 60 m. This provides growth of phytoplankton in the deepest layer (45-60 m), where nutrients are available.

Two different maxima of *Chl* are observed in summer. First, small and relatively shallow occupies thin 5 m layer at the depth of 20-20 m in June. This peak is situated in the lower zone of the coccolithophore bloom, which early summer maximum peak is observed at the same time. The coincidence in timing and intensity of June *Chl* peak and coccolithophores bloom evidences that these events may be related. Second, significantly stronger summer maximum is observed in August. Its intensity and vertical position have high interannual variability. The possible physical reason of this peak is intensifying in summer eddy-induced horizontal advection and vertical entrainment of nutients during summer wind bursts. This peak was exceptionally high in 2015, which was related to the impact of several storms in August, 2015.

In September-October the column-averaged *Chl* decreases, probably, due to the consumption of summer phytoplankton by mesozooplankthon having a seasonal maximum at the same time. During this period *Chl* decreases in the deeper layers and increases in the mixed layer, which is associated with the entrainment of the phytoplankton from summer subsurface maximum.

In November, when mixing deepens to upper boundary of nutricline the late autumn-early winter bloom of phytoplankton occupying the whole mixed\photic layer begins in the Black Sea reaching its maximum in December-January.

Acknowledgements

Seasonal variability of the vertical distribution of *Chl* was investigated with support of RSF, Russia, grant 19-77-00029. Analysis of the surface *Chl* variability was supported by RFBR, Russia, grant 17-05-41102 RGO_a. The data preparing and acquisition was made under FASO contract # 0827-2019-0002. Analysis of the seasonal *Chl* variability in relation to light attenuation was made under FASO contract # 0149-2019-0010.

Electronic Supplement

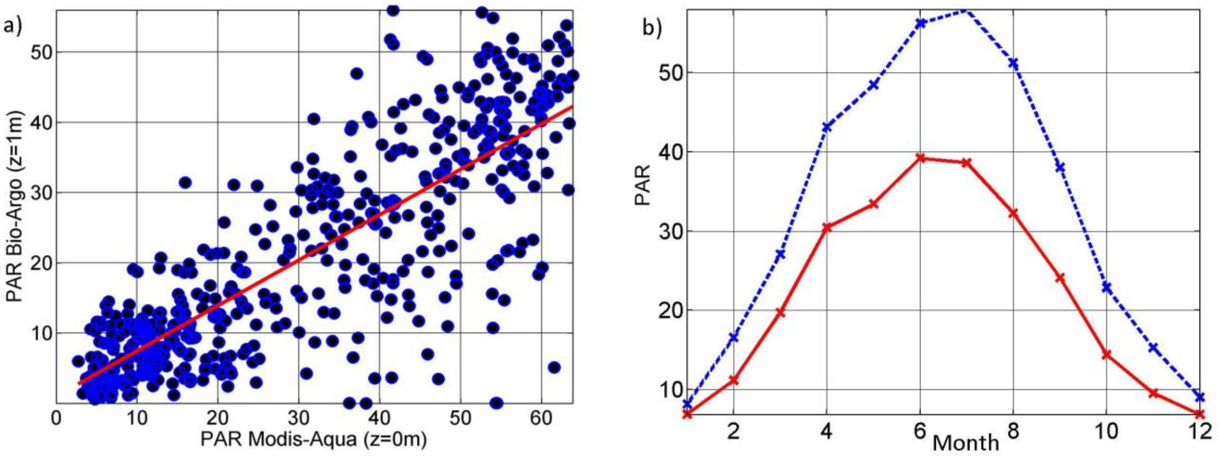

Fig. S1. a) Scatter diagramm of PAR from MODIS-Aqua and Qs (mol quanta m^{-2} d^{-1}) at 1 m depth measured by Bio-Argo floats; coefficient of correlation is equal to 0.82 b) Seasonal variability of PAR from MODIS-Aqua (blue line) and Qs (red line) at 1 m depth. For the comparison, MODIS measurements was interpolated on time and position of Bio-Argo data.

Literature

1. Alderkamp, A. C., de Baar, H. J., Visser, R. J., & Arrigo, K. R. (2010). Can photoinhibition control phytoplankton abundance in deeply mixed water columns of the Southern Ocean?. Limnology and Oceanography, 55(3), 1248-1264.
2. Alderkamp, A. C., Garcon, V., de Baar, H. J., & Arrigo, K. R. (2011). Short-term photoacclimation effects on photoinhibition of phytoplankton in the Drake Passage (Southern Ocean). Deep Sea Research Part I: Oceanographic Research Papers, 58(9), 943-955.
3. Azam, F., Fenchel, T., Field, J. G., Gray, J. S., Meyer-Reil, L. A., Thingstad, F. (1983). The ecological role of water- column microbes In the sea. Mar. Ecol. Prog. Ser. 10: 257-263.
4. Banse K. 2004. Should we continue to use the 1% light depth convention for estimating the compensation depth of phytoplankton for another 70 years? Limnol. Oceanogr. Bull. 13:49–52
5. Boss, E., & Behrenfeld, M. (2010). In situ evaluation of the initiation of the North Atlantic phytoplankton bloom. Geophysical Research Letters, 37(18).
6. Becquevort, S., Bouvier, T., Lancelot, C., Cauwet, G., Deliat, G., Egorov, V. N., & Popovichev, V. N. (2002). The seasonal modulation of organic matter utilization by bacteria in the Danube–Black Sea mixing zone. Estuarine, Coastal and Shelf Science,54(3), 337-354.

7. Berseneva, G. P., Churilova, T. Y., & Georgieva, L. V. (2004). Seasonal variability of the chlorophyll and phytoplankton biomass in the western part of the Black Sea. OCEANOLOGY, 44, 362-371.
8. Buitenhuis, E.T., Pangerc, T., Franklin, D.J., Le Quere, C., Malin, G. 2008. Growth rates of six coccolithophorid strains as a function of temperature. Limnology and Oceanography 53(3), 1181-1185.
9. Callieri, C., Slabakova, V., Dzhembekova, N., Slabakova, N., Peneva, E., Cabello-Yeves, P. J., Di Cesare, A., Eckert, E. M., Bertoni, R., Corno, G., Salcher, M. M., Kamburska, L., Bertoni, F., Moncheva, S. **(2019).** The mesopelagic anoxic Black Sea as an unexpected habitat for Synechococcus challenges our understanding of global “deep red fluorescence”. The ISME Journal | DOI: 10.1038/s41396-019-0378-z
10. Capet, A., Stanev, E., Beckers, J. M., Murray, J., & Grégoire, M. (2016). Decline of the Black Sea oxygen inventory. Biogeosciences, 13, 1287-1297.
11. Churilova, T., Suslin, V., Krivenko, O., Efimova, T., Moiseeva, N., Mukhanov, V., & Smirnova, L. (2017). Light absorption by phytoplankton in the upper mixed layer of the Black Sea: Seasonality and Parametrization. Frontiers in Marine Science, 4, 90.
12. Claustre, H., Bishop, J., Boss, E., Stewart, B., Berthon, J.-F., Coatanoan, C., Johnson, K., Lotiker, A., Ulloa, O., Perry, M.-J., D'Ortenzio, F., Hembise Fanton D’Andon, O. , Uitz, J. (2010) Bio-optical profiling floats as new observational tools for biogeochemical and ecosystem studieS. In: Hall, J., Harrison D.E. and Stammer, D. editor. Proceedings of the "OceanObs’09: Sustained Ocean Observations and Information for Society" Conference, Venice, Italy, 21-25 September 2009. 2: | DOI: 10.5270/OceanObs09.cwp.17
13. Cociasu, A., & Popa, L. (2004). Significant changes in Danube nutrient loads and their impact on the Romanian Black Sea coastal waters. Cercetari Marine,35, 25-37.
14. Cokacar, T., Oguz, T., & Kubilay, N. (2004). Satellite-detected early summer coccolithophore blooms and their interannual variability in the Black Sea. Deep Sea Research Part I: Oceanographic Research Papers, 51(8), 1017-1031.
15. Cullen, J. J. (2015). Subsurface Chlorophyll Maximum Layers: Enduring Enigma or Mystery Solved?. Annual Review of Marine Science, 7, 207-239.
16. Demidov, A. B. (1999). Spatial and temporal variability of chlorophyll a in the Black Sea during the winter-spring period. Oceanology, 39(5), 688-700.
17. Demidov, A. B. (2008). Seasonal dynamics and estimation of the annual primary production of phytoplankton in the Black Sea. Oceanology, 48(5), 664-678.
18. Durham, W. M., & Stocker, R. (2012). Thin phytoplankton layers: characteristics, mechanisms, and consequences. Annual review of marine science, 4, 177-207.

19. Eker-Develi, E., & Kideys, A. E. (2003). Distribution of phytoplankton in the southern Black Sea in summer 1996, spring and autumn 1998. Journal of Marine Systems, 39(3-4), 203-211.

20. Ferrari, R., Merrifield, S. T., & Taylor, J. R. (2015). Shutdown of convection triggers increase of surface chlorophyll. Journal of Marine Systems, 147, 116-122.

21. Finenko, Z. Z., Churilova, T. Y., Sosik, H. M., & Basturk, O. (2002). Variability of photosynthetic parameters of the surface phytoplankton in the Black Sea. Oceanology, 42(1), 53-67.

22. Finenko, Z. Z., Churilova, T. Y., & Lee, R. I. (2005). Dynamics of the vertical distributions of chlorophyll and phytoplankton biomass in the Black Sea. Oceanology, 45, S112.

23. Finenko, Z. Z., N. Hoepffner, R. Williams, S. A. Piontkovski. 2003. Phytoplankton carbon to chlorophyll a ratio: response to light, temperature and nutrient. Marine ecological journal/Morskoj ehkologicheskij zhurnal, 2003, 2(2), 40-64 (in Russian).

24. Finenko, Z., V. Suslin, I. Kovaleva. 2014. Seasonal and long-term dynamics of the chlorophyll concentration in the Black Sea according to satellite observations. Oceanology, 2014, 54, 596–605.

25. Ginzburg, A. I., Kostianoy, A. G., Nezlin, N. P., Soloviev, D. M., & Stanichny, S. V. (2002). Anticyclonic eddies in the northwestern Black Sea. Journal of Marine Systems, 32(1), 91-106.

26. Gran, H. H., & Braarud, T. (1935). A quantitative study of the phytoplankton in the Bay of Fundy and the Gulf of Maine (including observations on hydrography, chemistry and turbidity). Journal of the Biological Board of Canada, 1(5), 279-467.

27. Ilyin Yu.N., Belokopytov V.N. (2005) Seasonal and interannual variability of the parameters of the cold intermediate layer in the region of the Sevastopol anticyclonic eddy. Ecological safety of coastal and shelf zones and comprehensive use of shelf resources, 12, 29-40.

28. Ivanov, V. A., & Belokopytov, V. N. (2013). Oceanography of the Black Sea. ECOSY-Gidrofizika.

29. Kara, A. B., Helber, R. W., Boyer, T. P., & Elsner, J. B. (2009). Mixed layer depth in the Aegean, Marmara, Black and Azov Seas: Part I: general features. Journal of Marine Systems, 78, S169-S180.

30. Karageorgis, A. P., Gardner, W. D., Mikkelsen, O. A., Georgopoulos, D., Ogston, A. S., Assimakopoulou, G., ... & Pagou, K. (2014). Particle sources over the Danube River delta, Black Sea based on distribution, composition and size using optics, imaging and bulk analyses. Journal of Marine Systems, 131, 74-90.

31. Konovalov, S. K., & Murray, J. W. (2001). Variations in the chemistry of the Black Sea on a time scale of decades (1960–1995). Journal of Marine Systems, 31(1), 217-243.

32. Konovalov, S. K., Murray, J. W., & Luther III, G. W. (2005). Black Sea Biogeochemistry. Oceanography, 18(2), 24.

33. Krivenko O.V. The vertical distribution of chlorophyll fluorescence in the Black Sea during the warm period // Marine Ecological Journal, 2010, No. 2, V. 9, p. 5-21 (in Russian)

34. Krivenko, O.V., & Parkhomenko, A.V. (2010). Temporal and spatial variability of phytoplankton biomass in the Black Sea from 1948 to 2001 No. 4, V. 9, p. 5-23 (in Russian)

35. Kopelevich, O. V., Sheberstov, S. V., Yunev, O., Basturk, O., Finenko, Z. Z., Nikonov, S., & Vedernikov, V. I. (2002). Surface chlorophyll in the Black Sea over 1978–1986 derived from satellite and in situ data. Journal of marine systems, 36(3), 145-160.

36. Korchemkina, E. N., & Lee, M. E. (2014). Anomalous optical characteristics of the coastal waters of the Black Sea in July 2012 and their relation to the concentration of mineral suspended matter in water. Marine Hydrophysical Journal, 2, 39-43.

37. Kovalev, A. V., Mazzocchi, M. G., Kideyş, A. E., Toklu, B., & Skryabin, V. A. (2003). Seasonal Changes in the Composition and Abundance of Zooplankton in the Seas of the Mediterranean Basin. Turkish Journal of Zoology, 27(3), 205-219.

38. Kubryakov, A. A., & Stanichny, S. V. (2015a). Seasonal and interannual variability of the Black Sea eddies and its dependence on characteristics of the large-scale circulation. Deep Sea Research Part I: Oceanographic Research Papers, 97, 80-91

39. Kubryakov, A. A., & Stanichny, S. V. (2015b). Mesoscale eddies in the Black Sea from satellite altimetry data. Oceanology, 55(1), 56-67.

40. Kubryakov, A. A., Stanichny, S. V., Zatsepin, A. G., & Kremenetskiy, V. V. (2016). Long-term variations of the Black Sea dynamics and their impact on the marine ecosystem. Journal of Marine Systems, 163, 80-94.

41. Kubryakov A.A., Stanichny S.V. Seasonal and interannual chlorophyll A variability in the Black Sea from satellite and bio-argo measurements, 41st CIESM (Mediterranean Science Commission) Congress, 12-16 September, 2016, Kiel, Germany

42. Kubryakov, A. A., Stanichny, S. V., & Zatsepin, A. G. (2018). Interannual variability of Danube waters propagation in summer period of 1992–2015 and its influence on the Black Sea ecosystem. Journal of Marine Systems, 179, 10-30.

43. Kubryakov, A. A., Bagaev, A. V., Stanichny, S. V., & Belokopytov, V. N. (2018). Thermohaline structure, transport and evolution of the Black Sea eddies from hydrological and satellite data. Progress in oceanography, 167, 44-63.

44. Kubryakov, A. A., Zatsepin, A. G., & Stanichny, S. V. (2019a). Anomalous summer-autumn phytoplankton bloom in the Black Sea driven by several strong wind events. Journal of Marine Systems.

45. Kubryakov, A. A., Mikaelyan, A. S., & Stanichny, S. V. (2019b). Summer and winter coccolithophore blooms in the Black Sea and their impact on production of dissolved organic matter from Bio-Argo data. Journal of Marine Systems, 199, 103220.

46. Kubryakov A.A., Stanichny S.V., Belokopytov V.N., Zatsepin A.G., Piotukh V.B. (2019c) Variability of the thickness of the mixed layer in the Black Sea and its relationship with water dynamics and atmospheric effects. Physical Oceanography. 2019.Vol. 35, No. 5. P. 233–247. doi: 10.22449 / 0233-7584-2019-5-233-247

47. Kubryakova E. A. Korotaev G. K., Influence of Vertical Motions on Maintaining the Nitrate Balance in the Black Sea based on Numerical Simulation, Oceanology, 2016, Vol. 56, No. 1, pp. 25–35

48. Latasa, M., Estrada, M. and Delgado, M. (1992). Plankton-pigment relationships in the Northwestern Mediterranean during stratification. Mar. Ecol. Prog. Ser., 88(1), 61-73.

49. Lee, M. E., Shibanov, E. B., Korchemkina, E. N., & Martynov, O. V. (2015). Retrieval of seawater components’ concentration from upwelling radiation spectrum. Physical Oceanography, (6 (186)). (In Russian)

50. Lee, M. E., Shybanov, E. B., Korchemkina, E. N., & Martynov, O. V. (2016, November). Retrieval of concentrations of seawater natural components from reflectance spectrum. In 22nd International Symposium on Atmospheric and Ocean Optics: Atmospheric Physics (Vol. 10035, p. 100352Y). International Society for Optics and Photonics.

51. Langdon, C. (1988). On the causes of interspecific differences in the growth-irradiance relationship for phytoplankton. II. A general review. Journal of Plankton Research, 10(6), 1291-1312.

52. Letelier, R. M., Karl, D. M., Abbott, M. R., & Bidigare, R. R. (2004). Light driven seasonal patterns of chlorophyll and nitrate in the lower euphotic zone of the North Pacific Subtropical Gyre. Limnology and Oceanography, 49(2), 508-519.

53. Marra, J. F., Lance, V. P., Vaillancourt, R. D., & Hargreaves, B. R. (2014). Resolving the ocean's euphotic zone. Deep Sea Research Part I: Oceanographic Research Papers, 83, 45-50.

54. Mankovsky, V. I., Tolkachenko, G. A., Shibanov, E. B., Martynov, O. V., Korchemkina, E. N., Yakovleva, D. V., & Kalinsky, I. A . (2010). Optical characteristics of coastal waters and the atmosphere in the region of the Southern coast of Crimea at the end of the summer season of 2008. Marine Hydrophysical Journal, (3), pp. 52-74 (In Russian)

55. McQuatters-Gollop, A., Mee, L. D., Raitsos, D. E., & Shapiro, G. I. (2008). Non-linearities, regime shifts and recovery: The recent influence of climate on Black Sea chlorophyll. Journal of Marine Systems, 74(1), 649-658.

56. Mikaelyan, A. S. (1997). Long-term variability of phytoplankton communities in open Black Sea in relation to environmental changes. In Sensitivity to change: Black Sea, Baltic Sea and North Sea (pp. 105-116). Springer, Dordrecht.

57. Mikaelyan, A. S., Pautova, L. A., Pogosyan, S. I., & Sukhanova, I. N. (2005). Summer bloom of coccolithophorids in the northeastern Black Sea. Oceanology, 45, S127.

58. Mikaelyan, A. S., Zatsepin, A. G., & Chasovnikov, V. K. (2013). Long-term changes in nutrient supply of phytoplankton growth in the Black Sea. Journal of Marine Systems, 117, 53-64.

59. Mikaelyan, A. S., Pautova, L. A., Chasovnikov, V. K., Mosharov, S. A., & Silkin, V. A. (2015). Alternation of diatoms and coccolithophores in the north-eastern Black Sea: a response to nutrient changes. Hydrobiologia, 755(1), 89-105.

60. Mikaelyan, A.S., Chasovnikov, V.K., Kubryakov, A.A., Stanichny, S.V., 2017a. Phenology and drivers of the winter-spring phytoplankton bloom in the open Black Sea: the application of Sverdrup's hypothesis and its refinements. Prog. Oceanogr. 151:163–176.

61. Mikaelyan, A.S., G. I. Shapiro, V. K. Chasovnikov, F. Wobus, M. Zanacchi. 2017b. Drivers of the autumn phytoplankton development in the open Black Sea. *Journal of Marine Systems*, 174, 1–11. doi.org/10.1016/j.jmarsys.2017.05.006.

62. Mikaelyan, A. S., Zatsepin, A. G., & Chasovnikov, V. K. (2013). Long-term changes in nutrient supply of phytoplankton growth in the Black Sea. Journal of Marine Systems, 117, 53-64.

63. Mikaelyan, A. S., Kubryakov, A. A., Silkin, V. A., Pautova, L. A., & Chasovnikov, V. K. (2018). Regional climate and patterns of phytoplankton annual succession in the open waters of the Black Sea. Deep Sea Research Part I: Oceanographic Research Papers, 142, 44-57.

64. Nelson, D.M., Smith, Jr.,W.O., 1991. Sverdrup revisited: critical depths, maximum chlorophyll levels, and the control of Southern Ocean productivity by the irradiance mixing regime. Limnol. Oceanogr. 38 (8), 1650–1661. Doi.org/10.4319/lo.1991.36.8.1650.

65. Nezlin, N. P. (2006). Seasonal and interannual variability of remotely sensed chlorophyll. In The Black Sea Environment (pp. 333-349). Springer Berlin Heidelberg.

66. Oguz, T., Deshpande, A. G., & Malanotte-Rizzoli, P. (2002). The role of mesoscale processes controlling biological variability in the Black Sea coastal waters: inferences from

SeaWIFS-derived surface chlorophyll field. Continental Shelf Research, 22(10), 1477-1492.

67. Oguz, T., Dippner, J. W., & Kaymaz, Z. (2006). Climatic regulation of the Black Sea hydro-meteorological and ecological properties at interannual-to-decadal time scales. Journal of Marine Systems, 60(3), 235-254.
68. O'Reilly, J. E., Maritorena, S., Mitchell, B. G., Siegel, D. A., Carder, K. L., Garver, S. A., ... & McClain, C. (1998). Ocean color chlorophyll algorithms for SeaWiFS. Journal of Geophysical Research: Oceans, 103(C11), 24937-24953.
69. Organelli, E., Claustre, H., Bricaud, A., Barbieux, M., Uitz, J., D'Ortenzio, F., & Dall'Olmo, G. (2017). Bio-optical anomalies in the world's oceans: An investigation on the diffuse attenuation coefficients for downward irradiance derived from Biogeochemical Argo float measurements. Journal of Geophysical Research: Oceans, 122(5), 3543-3564.
70. Pakhomova, S., Vinogradova, E., Yakushev, E., Zatsepin, A., Shtereva, G., Chasovnikov, V., & Podymov, O. (2014). Interannual variability of the Black Sea proper oxygen and nutrients regime: the role of climatic and anthropogenic forcing. Estuarine, Coastal and Shelf Science, 140, 134-145.
71. Paasche, E. 2001. A review of the coccolithophorid Emiliania huxleyi (Prymnesiophyceae), with particular reference to growth, coccolith formation, and calcification-photosynthesis interactions. Phycologia 40(6), 503-529.
72. Pautova, L. A., Mikaelyan, A. S., & Silkin, V. A. (2007). Structure of plankton phytocoenoses in the shelf waters of the northeastern Black Sea during the Emiliania huxleyi bloom in 2002-2005. Oceanology, 47(3), 377.
73. Richardson, B. 2009. Physiological characteristics and competitive strategies of bloom-forming cyanobacteria and diatoms in Florida Bay. Contributions in Marine Science, 38, 19-36.
74. Shapiro, G. I., Stanichny, S. V., & Stanychna, R. R. (2010). Anatomy of shelf–deep sea exchanges by a mesoscale eddy in the North West Black Sea as derived from remotely sensed data. Remote Sensing of Environment, 114(4), 867-875.
75. Silkin, V. A., Pautova, L. A., Pakhomova, S. V., Lifanchuk, A. V., Yakushev, E. V., & Chasovnikov, V. K. (2014). Environmental control on phytoplankton community structure in the NE Black Sea. Journal of Experimental Marine Biology and Ecology, 461, 267-274.
76. Siegel, D. A., Doney, S. C., & Yoder, J. A. (2002). The North Atlantic spring phytoplankton bloom and Sverdrup's critical depth hypothesis. Science, 296(5568), 730-733.

77. Silkin, V. A., Pautova, L. A., Giordano, M., Chasovnikov, V. K., Vostokov, S. V., Podymov, O. I., ... & Moskalenko, L. V. (2019). Drivers of phytoplankton blooms in the northeastern Black Sea. Marine pollution bulletin, 138, 274-284.

78. Sorokin, Y. U. I. (1983). The Black Sea.

79. Stelmakh L. V., Babic I. I. (2006). Seasonal variability of the organic carbon to chlorophyll "a" ratio and factors its determining in phytoplankton of coastal waters of the Black Sea. Marine Biological Journal, №2, V.5, pp. 74-87.

80. Stelmakh L. V, Mansurova I. M. Ecological and physiological basis of phytoplankton biodiversity in the Black Sea // Optimization and Protection of Ecosystems. Simferopol: TNU, 2012. Iss. 7. P. 149–158.

81. Stanev, E. V., He, Y., Grayek, S., & Boetius, A. (2013). Oxygen dynamics in the Black Sea as seen by Argo profiling floats. Geophysical Research Letters, 40(12), 3085-3090.

82. Stanev, E. V., Grayek, S., Claustre, H., Schmechtig, C., & Poteau, A. (2017). Water intrusions and particle signatures in the Black Sea: a Biogeochemical-Argo float investigation. Ocean Dynamics, 67(9), 1119-1136.

83. Stanev, E. V., Poulain, P. M., Grayek, S., Johnson, K. S., Claustre, H., & Murray, J. W. (2018). Understanding the Dynamics of the Oxic-Anoxic Interface in the Black Sea. Geophysical Research Letters.

84. Sverdrup, H. U. (1953). On vernal blooming of phytoplankton. Journal Conseil Exp Mer, 18, 287-295.

85. Sur, H. İ., Ilyin, Y. P., Özsoy, E., & Ünlüata, Ü. (1996). The impacts of continental shelf/deep water interactions in the Black Sea. J. mar. Sys, 7, 293-320.

86. Taylor, J. R., & Ferrari, R. (2011). Shutdown of turbulent convection as a new criterion for the onset of spring phytoplankton blooms. Limnology and Oceanography, 56(6), 2293-2307.

87. Titov, V. B., 2004. Formation of the upper convective layer and the cold intermediate layer in the Black Sea in relation to the winter severity. Oceanology 44: 327–330.

88. Tuğrul, S., Murray, J. W., Friederich, G. E., & Salihoğlu, İ. (2014). Spatial and temporal variability in the chemical properties of the oxic and suboxic layers of the Black Sea. Journal of Marine Systems, 135, 29-43.

89. Tyrrell, T., & Merico, A. (2004). Emiliania huxleyi: bloom observations and the conditions that induce them. In Coccolithophores (pp. 75-97). Springer Berlin Heidelberg.

90. Vedernikov, V. I., & Demidov, A. B. (1993). Primary Production And Chlorophyll In The Deep Regions Of The Black-Sea. Okeanologiya, 33(2), 229-235.

91. Vedernikov, V. I., & Demidov, A. B. (1997). Vertical distribution of primary production and chlorophyll during different seasons in deep regions of the Black Sea. Oceanology, 37(3), 376-384.

92. Vinogradov, M. E., Shushkina, E. A., Mikaelyan, A. S., & Nezlin, N. P. (1999). Temporal (seasonal and interannual) changes of ecosystem of the open waters of the Black Sea. In Environmental Degradation of the Black Sea: Challenges and Remedies (pp. 109-129). Springer, Dordrecht.

93. Vladimirov, V. L., Mankovsky, V. I., Solov'ev, M. V., & Mishonov, A. V. (1997). Seasonal and long-term variability of the Black Sea optical parameters. InSensitivity to Change: Black Sea, Baltic Sea and North Sea (pp. 33-48). Springer Netherlands.

94. Xing, X., Morel, A., Claustre, H., Antoine, D., D'Ortenzio, F., Poteau, A., & Mignot, A. (2011). Combined processing and mutual interpretation of radiometry and fluorimetry from autonomous profiling Bio-Argo floats: Chlorophyll a retrieval. Journal of Geophysical Research: Oceans, 116(C6).

95. Xing, X., Morel, A., Claustre, H., D'Ortenzio, F., & Poteau, A. (2012). Combined processing and mutual interpretation of radiometry and fluorometry from autonomous profiling Bio-Argo floats: 2. Colored dissolved organic matter absorption retrieval. Journal of Geophysical Research: Oceans, 117(C4).

96. Xing, X., Qiu, G., Boss, E., & Wang, H. (2019). Temporal and vertical variations of particulate and dissolved optical properties in the South China Sea. Journal of Geophysical Research: Oceans.

97. Yankovsky, A. E., Lemeshko, E. M., & Ilyin, Y. P. (2004). The influence of shelfbreak forcing on the alongshelf penetration of the Danube buoyant water, Black Sea. Continental shelf research, 24(10), 1083-1098.

98. Yunev, O. A., Vedernikov, V. I., Basturk, O., Yilmaz, A., Kideys, A. E., Moncheva, S., & Konovalov, S. K. (2002). Long-term variations of surface chlorophyll a and primary production in the open Black Sea. Marine ecology progress series,230, 11-28.

99. Yunev, O. A., Moncheva, S., & Carstensen, J. (2005). Long-term variability of vertical chlorophyll a and nitrate profiles in the open Black Sea: eutrophication and climate change. Marine Ecology Progress Series, 294, 95-107.

100. Yunev, O. A. (2011). Eutrophication and annual primary production of phytoplankton in the deep-water part of the Black Sea. Oceanology, 51(4), 616.

101. Zatsepin, A. G., Kremenetskiy, V. V., Poyarkov, S. G., Ratner, Y. B., & Stanichny, S. V. (2002). Influence of wind field on water circulation in the Black Sea. Complex Investigation of the Northeastern Black Sea. Nauka, Moscow, 91-105

102. Zatsepin, A. G., Ginzburg, A. I., Kostianoy, A. G., Kremenetskiy, V. V., Krivosheya, V. G., Stanichny, S. V., & Poulain, P. M. (2003). Observations of Black Sea mesoscale eddies and associated horizontal mixing. Journal of Geophysical Research: Oceans (1978–2012), 108(C8).

103. Zatsepin A. G., Denisov E. S., Emel'yanov S. V., Kremenetskiy V. V., Poyarkov S. G., Stroganov O. Yu., Stanichnaya R. R., and Stanichny S. V (2005). Effect of bottom slope and wind on the near-shore current in a rotating stratified fluid: laboratory modeling for the Black Sea. Oceanology, 45(1), S13-S26

104. Zatsepin, A. G., Arashkevich, E. G., Kubryakov, A. A., Silkin, V. A., & Stanichny, S. V. (2017). Role Of Wind Exposure In Primary Product Support In The Black Sea Warm Period Of The Year. In The collection of abstracts of the fifteenth All-Russian open conference "Modern problems of remote sensing of the Earth from space" (pp. 251-251) (in Russian)

105. Zernova, V. V., & Nezlin, N. P. (1983). Seasonal Changes in the Phytocene of the Northeastern Part of the Black Sea in 1978. Sezonnye izmeneniya chernomorskogo planktona, 12-34.

106. Zhou, F., Shapiro, G., & Wobus, F. (2014). Cross-shelf exchange in the northwestern Black Sea. Journal of Geophysical Research: Oceans, 119(4), 2143-2164.

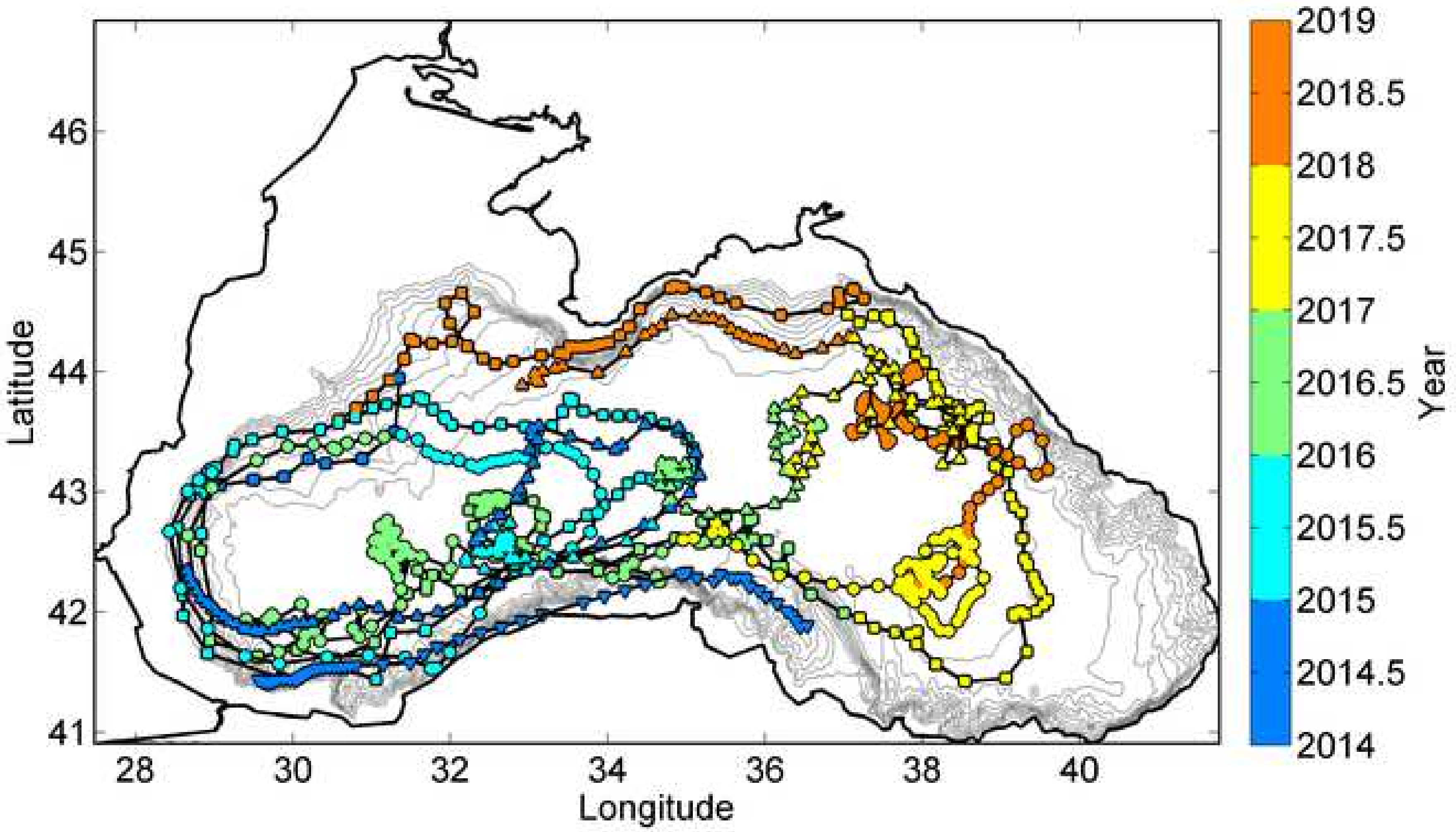
46
45
44
43
42
41
Latitude
28
30
32
34
36
38
40
Longitude
2019
2018.5
2018
2017.5
2017
2016.5
2016
2015.5
2015
2014.5
2014
Year

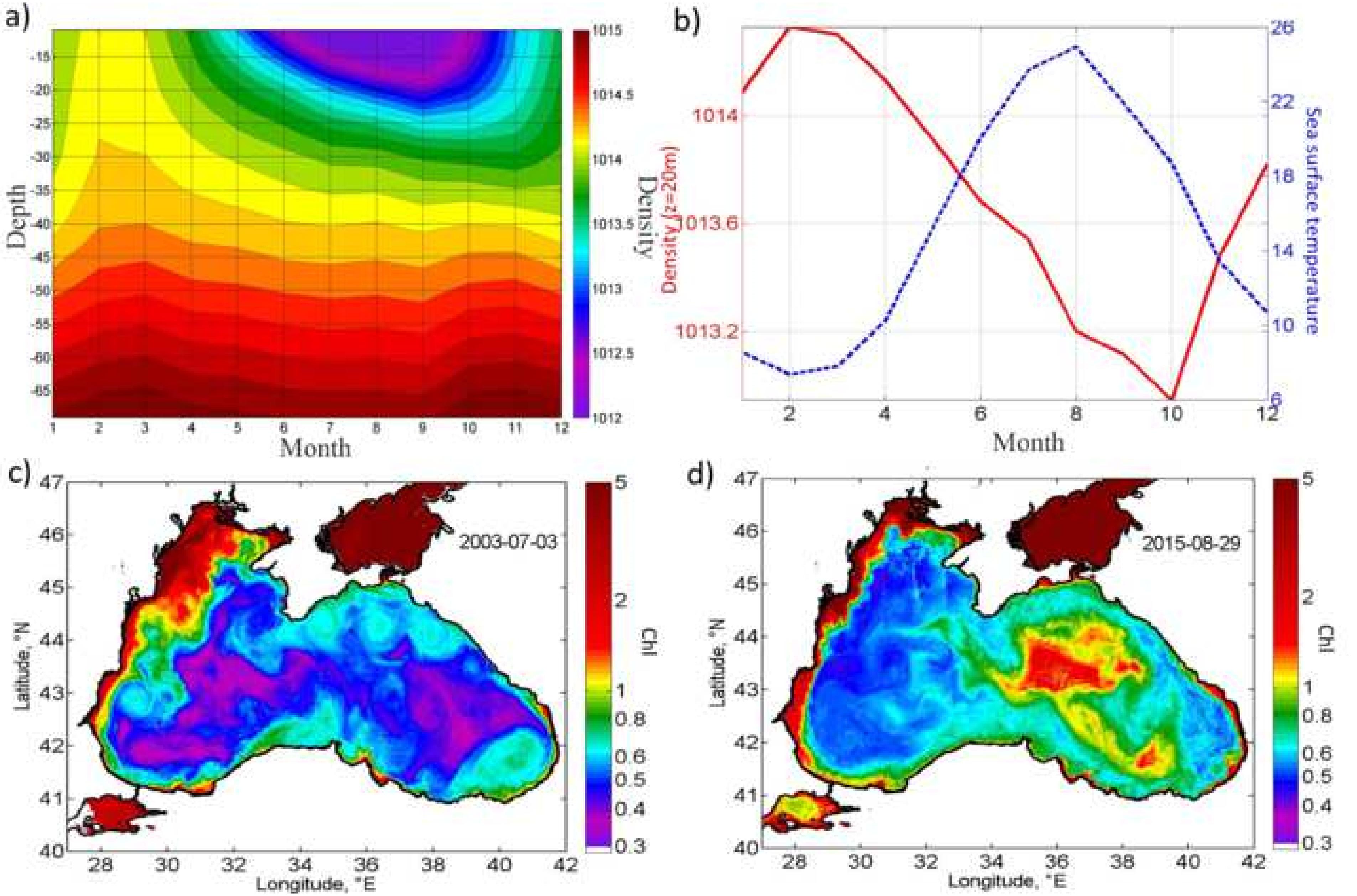
a)
Depth
-15
-20
-25
-30
-35
-40
-45
-50
-55
-60
-65
1
2
3
4
5
6
7
8
9
10
11
12
Month
1015
1014.5
1014
1013.5
1013
1012.5
1012
Density
b)
1014
1013.6
1013.2
Density (z=20m)
26
22
18
14
10
6
Sea surface temperature
2
4
6
8
10
12
Month
c)
2003-07-03
Latitude, °N
Longitude, °E
47
46
45
44
43
42
41
40
28
30
32
34
36
38
40
42
5
2
1
0.8
0.6
0.5
0.4
0.3
Chl
d)
2015-08-29
Latitude, °N
Longitude, °E
47
46
45
44
43
42
41
40
28
30
32
34
36
38
40
42
5
2
1
0.8
0.6
0.5
0.4
0.3
Chl

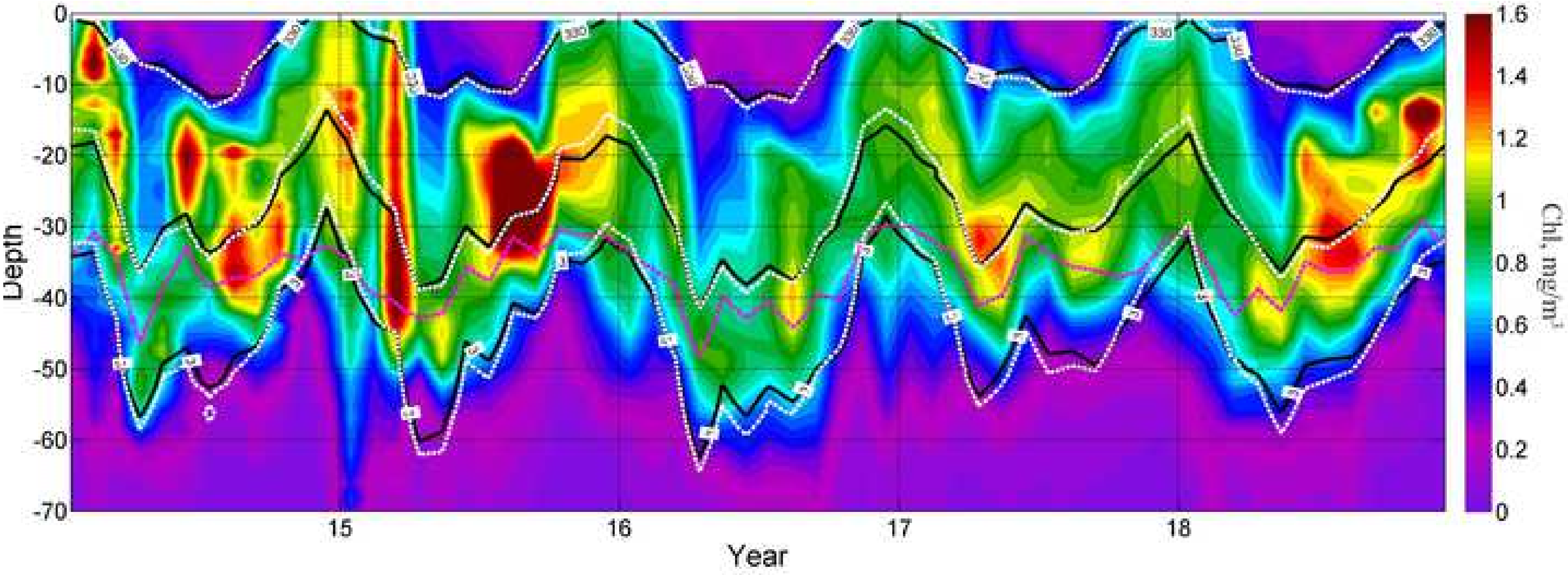
0
-10
-20
-30
-40
-50
-60
-70
Depth
15
16
17
18
Year
1.6
1.4
1.2
1
0.8
0.6
0.4
0.2
0
Chl, mg/m^3
330

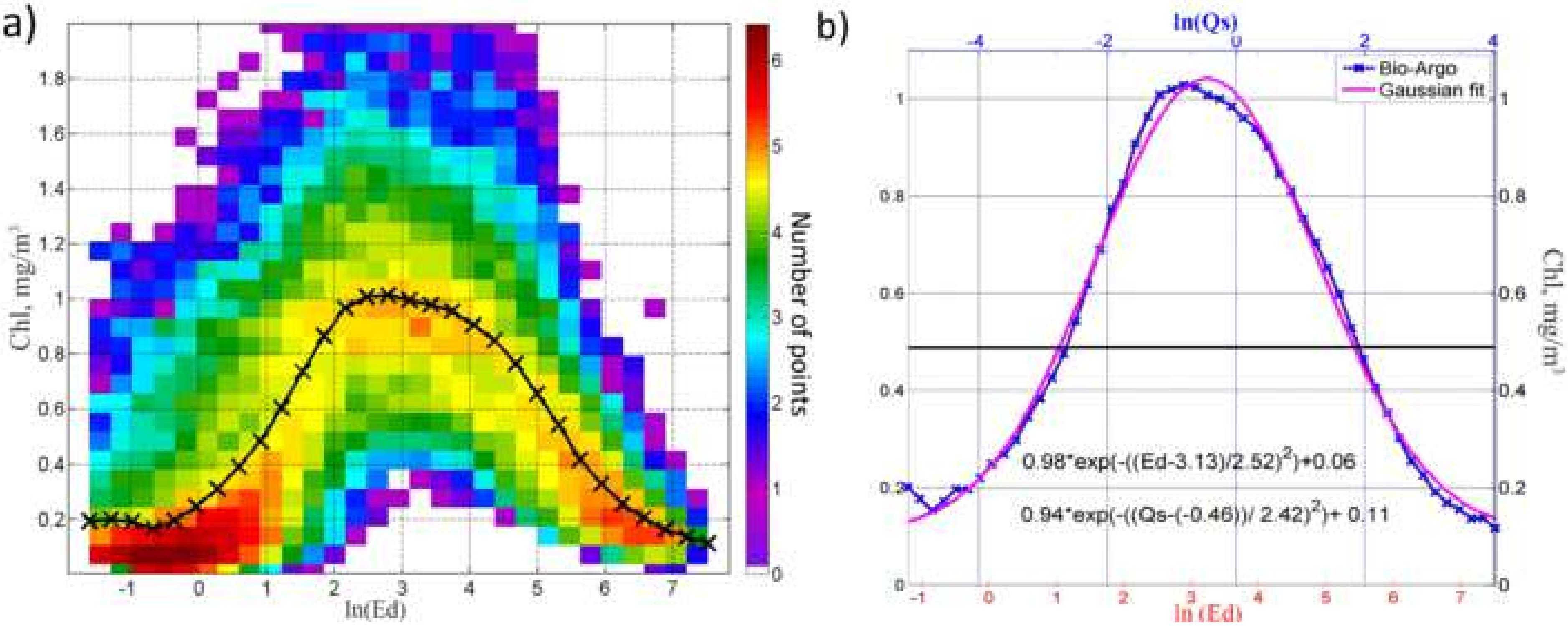
a)
Chl, mg/m³
1.8
1.6
1.4
1.2
1
0.8
0.6
0.4
0.2
-1
0
1
2
3
4
5
6
7
ln(Ed)
Number of points
6
5
4
3
2
1
0
b)
ln(Qs)
-4
-2
0
2
4
Bio-Argo
Gaussian fit
0.98*exp(-((Ed-3.13)/2.52)²)+0.06
0.94*exp(-((Qs-(-0.46))/ 2.42)²)+ 0.11
Chl, mg/m³
ln (Ed)

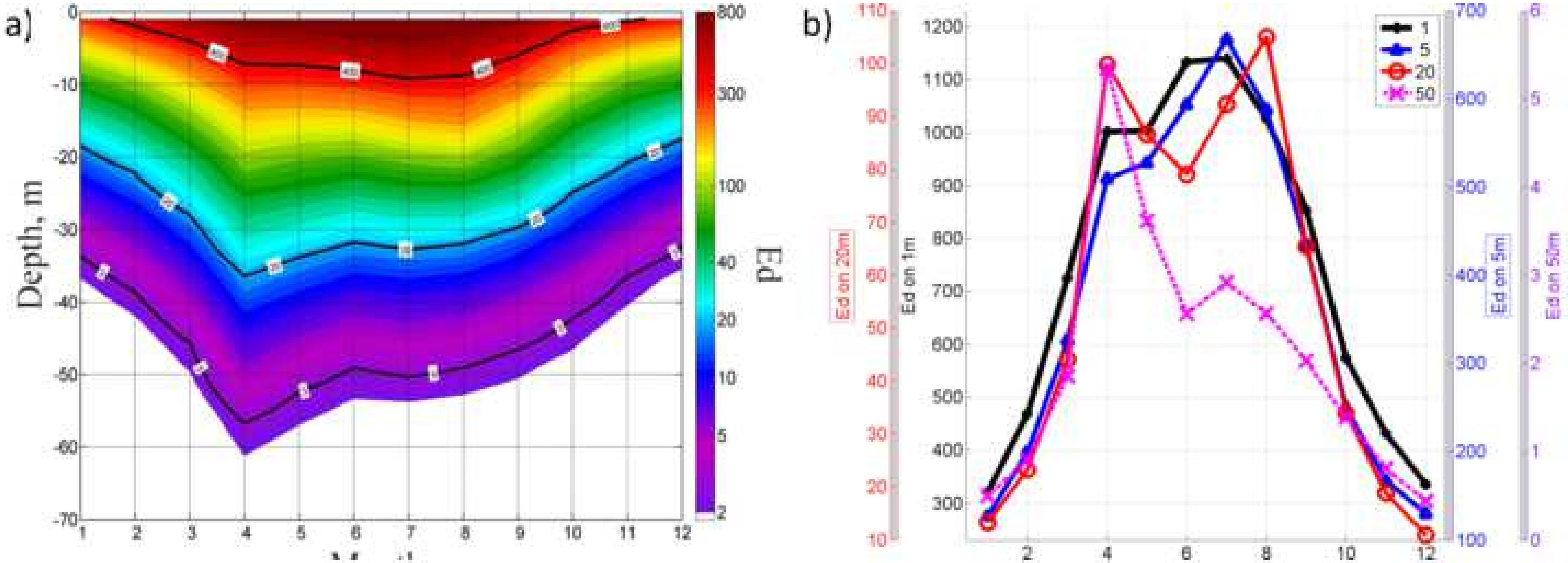
a)
Depth, m
0
-10
-20
-30
-40
-50
-60
-70
1
2
3
4
5
6
7
8
9
10
11
12
800
300
100
40
20
10
5
2
Ed
b)
Ed on 20m
110
100
90
80
70
60
50
40
30
20
10
Ed on 1m
1200
1100
1000
900
800
700
600
500
400
300
2
4
6
8
10
12
1
5
20
50
Ed on 5m
700
600
500
400
300
200
100
Ed on 50m
6
5
4
3
2
1
0

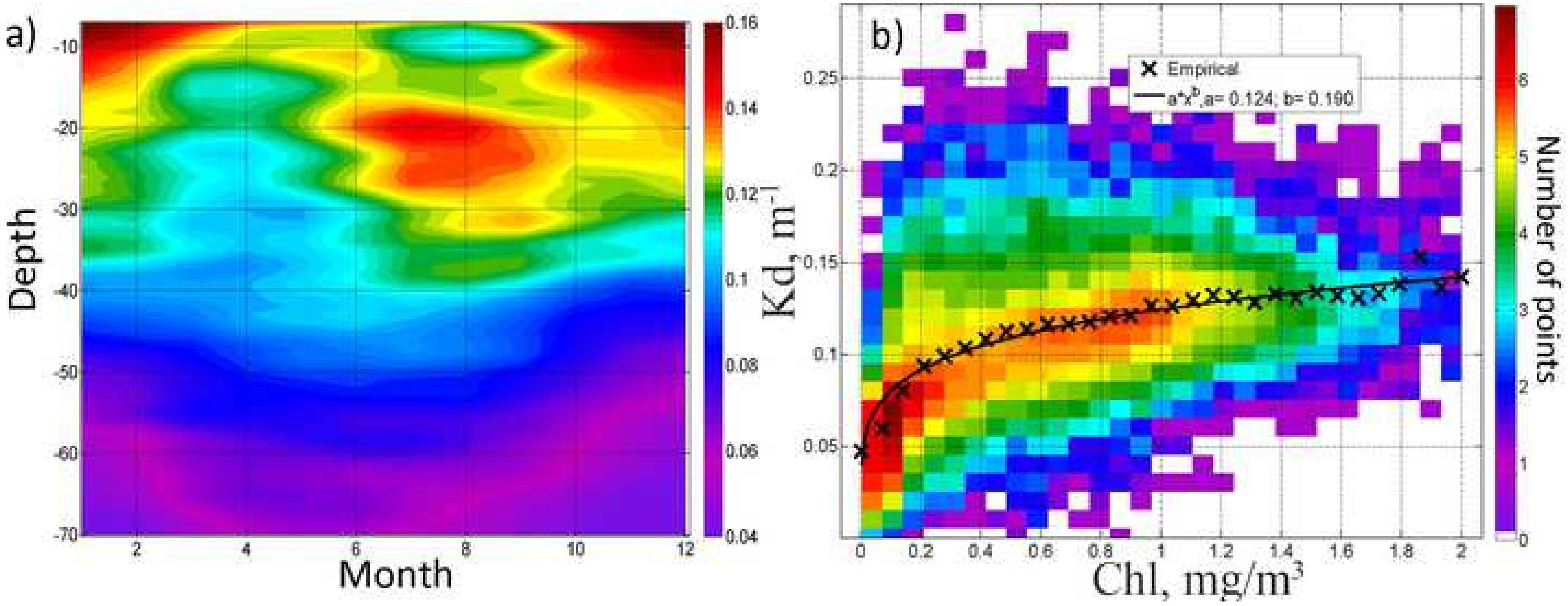
a)
Depth
-10
-20
-30
-40
-50
-60
-70
Month
2
4
6
8
10
12
0.16
0.14
0.12
0.1
0.08
0.06
0.04
b)
Kd, m⁻¹
0.25
0.2
0.15
0.1
0.05
Chl, mg/m³
0
0.2
0.4
0.6
0.8
1
1.2
1.4
1.6
1.8
2
Empirical
a*x^b,a= 0.124; b= 0.190
Number of points
6
5
4
3
2
1
0

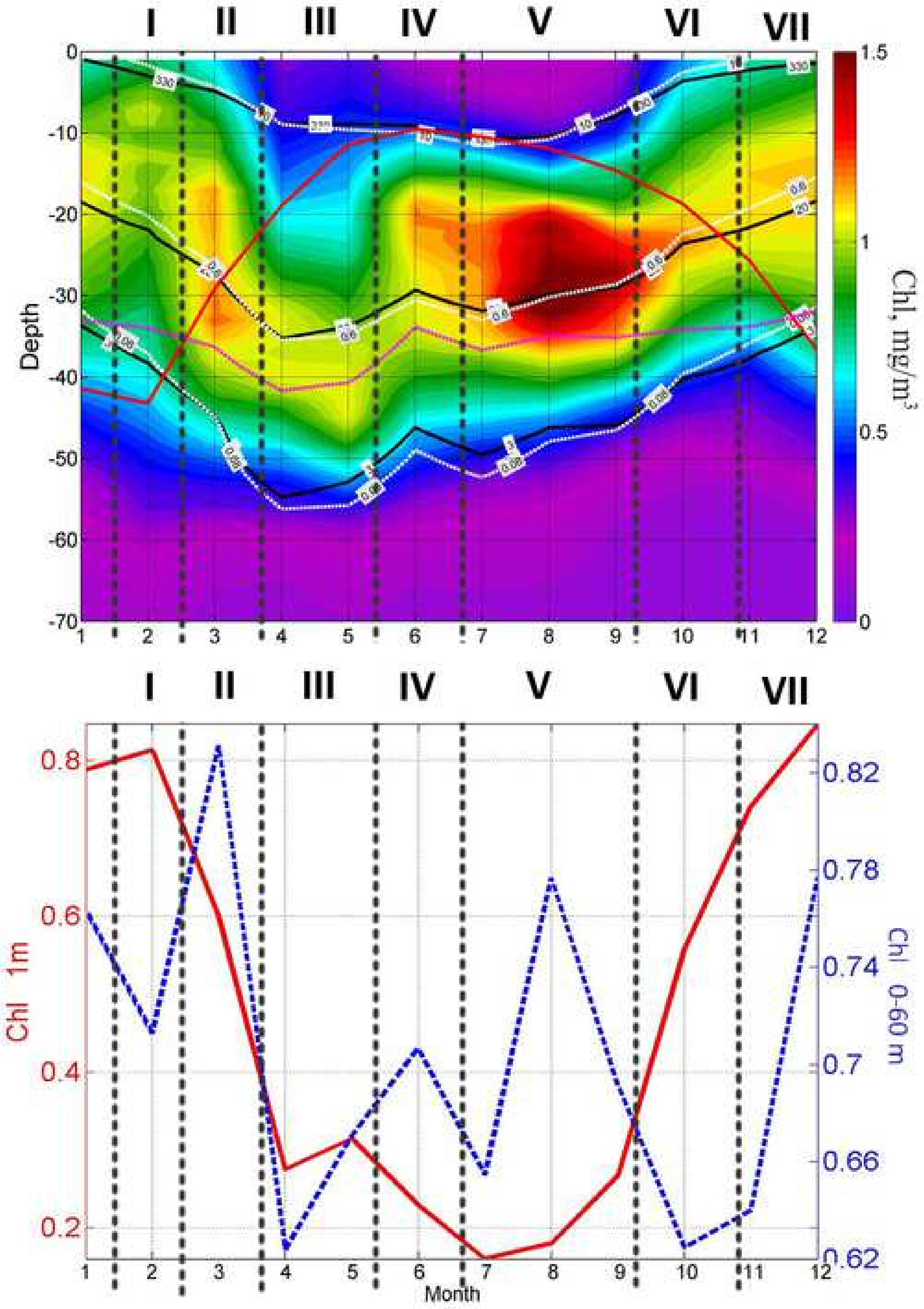
I
II
III
IV
V
VI
VII
Depth
0
-10
-20
-30
-40
-50
-60
-70
1
2
3
4
5
6
7
8
9
10
11
12
Chl, mg/m^3
1.5
1
0.5
0
330
10
20
0.8
0.08
Chl 1m
0.8
0.6
0.4
0.2
Chl 0-60 m
0.82
0.78
0.74
0.7
0.66
0.62
Month

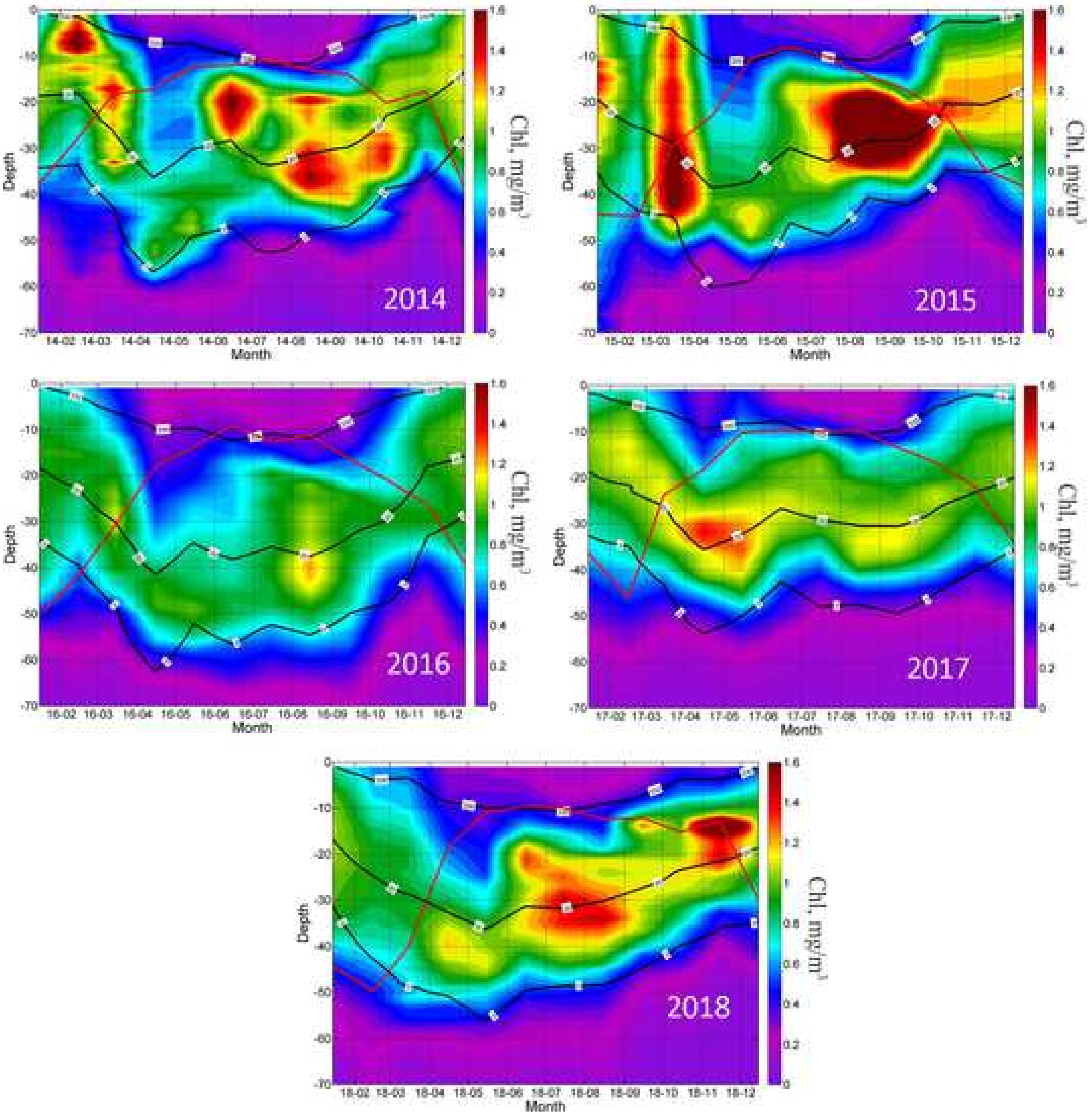
2014
2015
2016
2017
2018
Depth
Month
Chl, mg/m³
0
-10
-20
-30
-40
-50
-60
-70
0
0.2
0.4
0.6
0.8
1
1.2
1.4
1.6
14-02 14-03 14-04 14-05 14-06 14-07 14-08 14-09 14-10 14-11 14-12
15-02 15-03 15-04 15-05 15-06 15-07 15-08 15-09 15-10 15-11 15-12
16-02 16-03 16-04 16-05 16-06 16-07 16-08 16-09 16-10 16-11 16-12
17-02 17-03 17-04 17-05 17-06 17-07 17-08 17-09 17-10 17-11 17-12
18-02 18-03 18-04 18-05 18-06 18-07 18-08 18-09 18-10 18-11 18-12

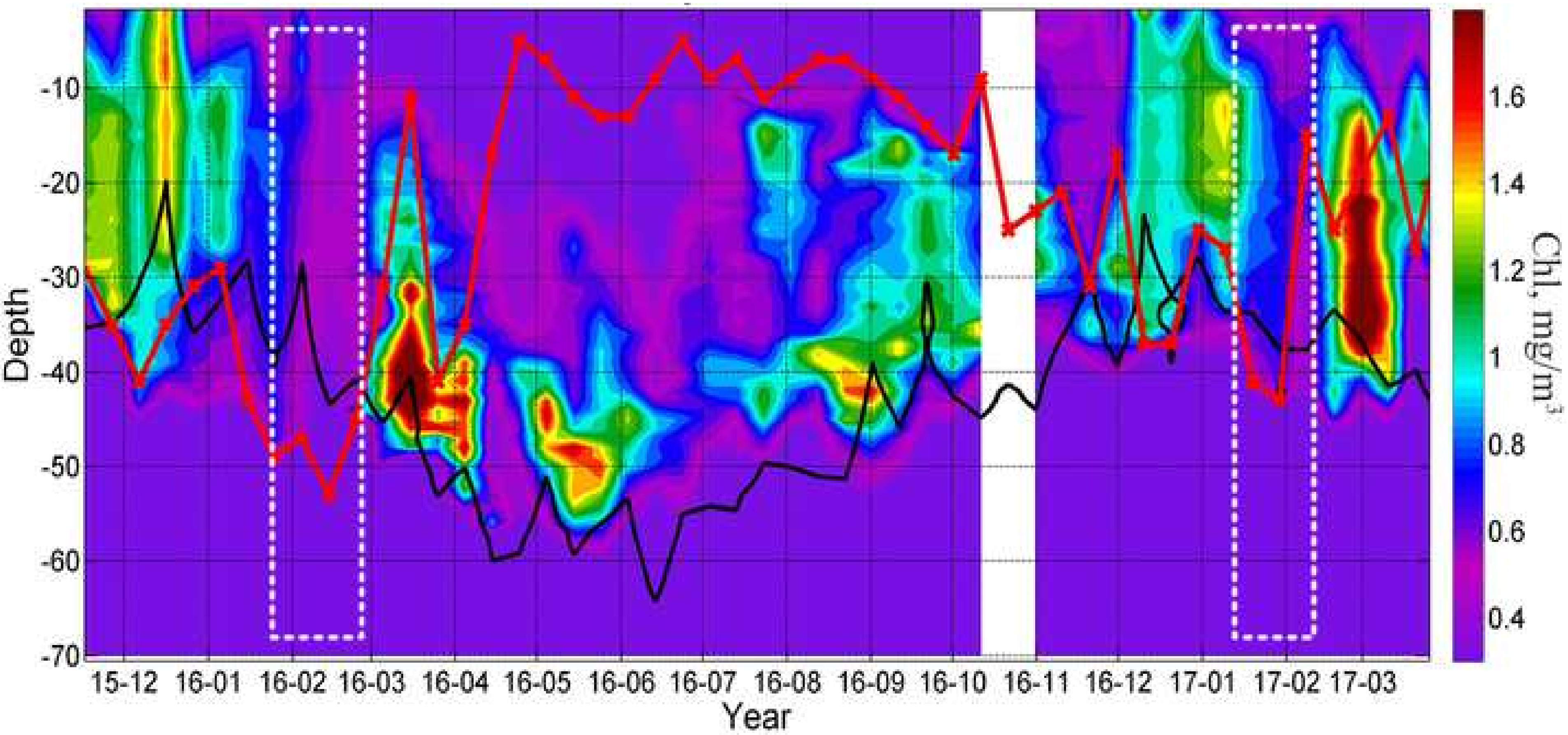
Depth
-10
-20
-30
-40
-50
-60
-70
15-12
16-01
16-02
16-03
16-04
16-05
16-06
16-07
16-08
16-09
16-10
16-11
16-12
17-01
17-02
17-03
Year
Chl, mg/m^3
1.6
1.4
1.2
1
0.8
0.6
0.4

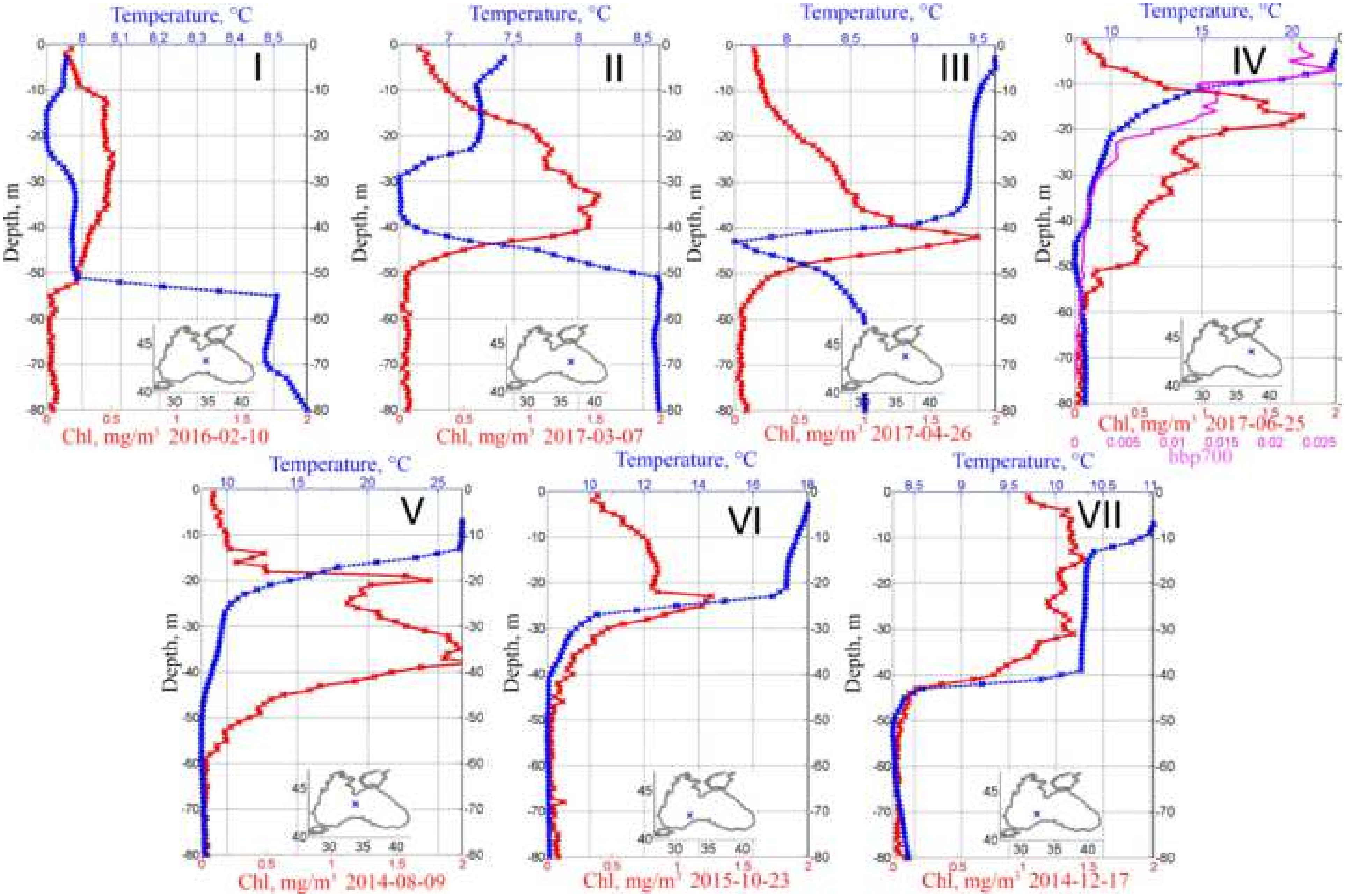
Temperature, °C
I
II
III
IV
V
VI
VII
Depth, m
Chl, mg/m³ 2016-02-10
Chl, mg/m³ 2017-03-07
Chl, mg/m³ 2017-04-26
Chl, mg/m³ 2017-06-25
bbp700
Chl, mg/m³ 2014-08-09
Chl, mg/m³ 2015-10-23
Chl, mg/m³ 2014-12-17
0
-10
-20
-30
-40
-50
-60
-70
-80
0.5
1
1.5
2
0.005
0.01
0.015
0.02
0.025
30
35
40
45

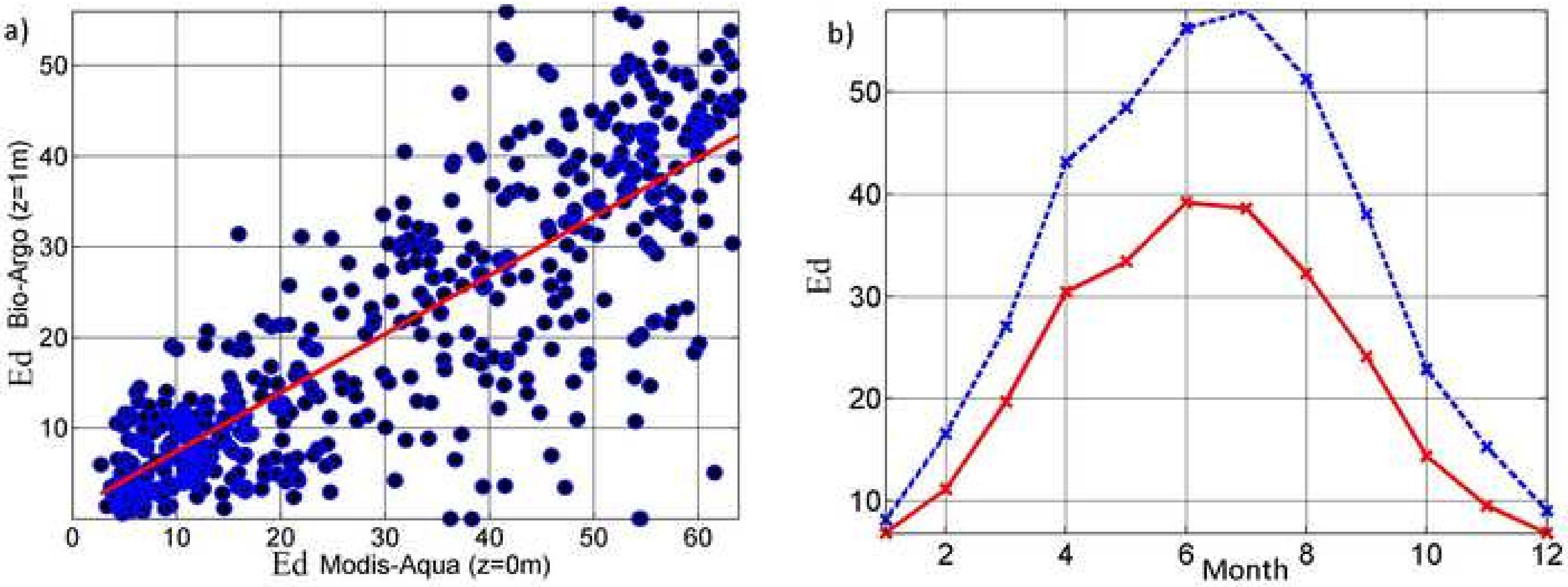
a)
Ed Bio-Argo (z=1m)
10
20
30
40
50
0
10
20
30
40
50
60
Ed Modis-Aqua (z=0m)
b)
Ed
10
20
30
40
50
2
4
6
8
10
12
Month